Available online at www.sciencedirect.com
SCIENCE DIRECT®
ELSEVIER
Life Sciences xx (2005) xxx – xxx
Life Sciences
www.elsevier.com/locate/lifescie

Effect of the difference in vehicles on gene expression in the rat liver—analysis of the control data in the Toxicogenomics Project Database

Kayoko Takashima [a], Yumiko Mizukawa [a,c], Katsumi Morishita [a], Manabu Okuyama [a], Toshihiko Kasahara [a], Naoki Toritsuka [a], Toshikazu Miyagishima [a,b], Taku Nagao [a], Tetsuro Urushidani [a,b,c,*]

[a] *Toxicogenomics Project, National Institute of Health Sciences, 1-18-1 Kamiyoga, Setagaya-Ku, Tokyo, 158-8501, Japan*
[b] *Present address of Toxicogenomics Project, National Institute of Biomedical Innovation, 7-6-8, Saito-Asagi, Ibaraki, Osaka, 567-0085, Japan*
[c] *Department of Pathophysiology, Faculty of Pharmaceutical Sciences, Doshisha Women's College of Liberal Arts, Kodo, Kyotanabe, Kyoto 610-0395, Japan*

Received 30 July 2005; accepted 1 November 2005

Abstract

The Toxicogenomics Project is a 5-year collaborative project by the Japanese government and pharmaceutical companies in 2002. Its aim is to construct a large-scale toxicology database of 150 compounds orally administered to rats. The test consists of a single administration test (3, 6, 9 and 24 h) and a repeated administration test (3, 7, 14 and 28 days), and the conventional toxicology data together with the gene expression data in liver as analyzed by using Affymetrix GeneChip are being accumulated. In the project, either methylcellulose or corn oil is employed as vehicle. We examined whether the vehicle itself affects the analysis of gene expression and found that corn oil alone affected the food consumption and biochemical parameters mainly related to lipid metabolism, and this accompanied typical changes in the gene expression. Most of the genes modulated by corn oil were related to cholesterol or fatty acid metabolism (e.g., CYP7A1, CYP8B1, 3-hydroxy-3-methylglutaryl-Coenzyme A reductase, squalene epoxidase, angiopoietin-like protein 4, fatty acid synthase, fatty acid binding proteins), suggesting that the response was physiologic to the oil intake. Many of the lipid-related genes showed circadian rhythm within a day, but the expression pattern of general clock genes (e.g., period 2, arylhydrocarbon nuclear receptor translocator-like, D site albumin promoter binding protein) were unaffected by corn oil, suggesting that the effects are specific for lipid metabolism. These results would be useful for usage of the database especially when drugs with different vehicle control are compared.

Keywords: Toxicogenomics; Vehicle control; Methylcellulose; Corn oil; Lipid metabolism; Rat; Liver

Introduction

The Toxicogenomics Project is a 5-year collaborative project by the National Institute of Health Sciences (NIHS) and 17 pharmaceutical companies in Japan which started in 2002 (Urushidani and Nagao, 2005). In April 2005, some rearrangements were made and now the project is conducted by NIHS, the National Institute of Biomedical Innovation, and 16 pharmaceutical companies. Its aim is to construct a large-scale toxicology database of transcriptome for prediction of toxicity of new chemical entities in the early stage of drug development. About 150 chemicals, mainly medicinal compounds, have been selected, and the following are examined for each. The in vivo test using rat consists of a single administration test (3, 6, 9 and 24 h with 4 dose levels including vehicle control) as well as a repeated administration test (3, 7, 14 and 28 days with 4 dose levels including vehicle control), and the data of body weight, general symptoms, histopathological examination of liver and kidney, and blood biochemistry are obtained from each animal. The gene expression in liver (and kidney in some cases) is comprehensively analyzed by using Affymetrix GeneChip. An in vitro test using rat and human hepatocytes is also carried out to accomplish the bridging between the species. By April 2005, more than 100 chemicals, covering wide medication categories, have been finished or are ongoing.

* Corresponding author. Department of Pathophysiology, Faculty of Pharmaceutical Sciences, Doshisha Women's College of Liberal Arts, Kodo, Kyotanabe, Kyoto 610-0395, Japan. Tel.: +81 0774 65 8689.
E-mail address: turushid@dwc.doshisha.ac.jp (T. Urushidani).

0024-3205/$ - see front matter © 2005 Published by Elsevier Inc.
doi:10.1016/j.lfs.2005.11.010

Along with the effects of the chemicals, a vast amount of control data is being accumulated.

The main purpose of the project is to predict toxicity in the early stage of drug development. The potential usefulness of microarray data for the estimation of toxicity of drugs makes it possible for this technology to be used in the late stage of development, i.e., application in the field of regulatory science. In this case, however, more strict and precise validation is needed in order to assure the reliability of the data. It is well known that a difference in the platform considerably effects a variation in the microarray data (Waring et al., 2004) and this is quite difficult to overcome. In our project, either methylcellulose or corn oil is employed as vehicle, according to the dispensability of the drug. It is quite possible that the difference in the vehicle control affects the analysis, as observed by multiple comparison of drug effects. In traditional toxicological study, comparison of the drug is exclusively made against its vehicle control. However, in the transcriptome database, it is usually necessary to make a comparison among various drugs by clustering or discriminant analysis. The history of this field is not old enough for collecting appropriate data regarding this issue. Our database enables us to make various comparisons among different vehicles, protocols, facilities, chip versions, etc. In this present report, we focus on the influence of vehicles on the control parameters including the gene expression profile in the rat liver as a basic study for future analysis.

Materials and methods

Animal treatment

Male Sprague-Dawley rats were purchased from Charles River Japan Inc., (Kanagawa, Japan) at 5-weeks of age. After a 7-day quarantine and acclimatization period, the animals were divided into groups of 5 animals using a computerized stratified random grouping method based on the body weight for each age. The animals were individually housed in stainless-steel cages in a room that was lighted for 12 h (7:00–19:00) daily, ventilated with an air-exchange rate of 15 times per hour, and maintained at 21–25 °C with a relative humidity of 40–70%. Each animal was allowed free access to water and pellet food (CRF-1, sterilized by radiation, Oriental Yeast Co., Japan).

According to the protocol in our project, rats in each group were orally administered with various drugs suspended or dissolved either in 0.5% methylcellulose solution or corn oil according to their dispersibility. Each drug had 4 different dose levels, including the vehicle control alone, which was exclusively analyzed in the present study. Drug treatment was performed between 9:00 and 11:30 a.m. For single-dose experiments, rats were sacrificed at 3, 6, 9, and 24 h after dosing. For repeated dose experiments, the animals were treated for 3, 7, 14 or 28 days, and they were sacrificed 24 h after the last dosing. Body weights were recorded every day while food consumption was recorded every 4 days during repeated dosing. Blood samples were collected upon sacrifice in tubes containing heparin lithium (blood biochemistry), EDTA-2K (hematology), or 1/9 vol of 3.8% citric acid (coagulation), and the following items were examined: hematology: the numbers of red blood cells, reticulocytes, white blood cells, eosinophils, monocytes, platelets, neutrophils, basophils, and lymphocytes, hemoglobin, mean red blood cell volume, mean hemoglobin contents, and mean hemoglobin concentration (Advia 120, Bayer); blood coagulation: prothorombin time, active partial prothrombin time, and fibrinogen (Sysmex CA-5000, Sysmex); and blood biochemistry: alkaline phosphatase, total cholesterol, triglyceride, phospholipid, total and direct bilirubin, glucose, blood urea nitrogen, creatinine, Na, K, Ca, Cl, inorganic phosphate, total protein, albumin, globulin/albumin ratio, aspartate aminoptansferase, alanine aminotransferase, lactate dehydrogenase, and γ-glutamyltranspeptidase, which were determined by an autoanalyzer (Hitachi 7080).

When the analysis was performed (April 2005), 65 compounds had been completed in 4 different contract research organizations. In order to eliminate the variations due to the difference in the facility, we selected a laboratory (Japan Bioassay Center, Kanagawa, Japan) where at least 7 experiments for each vehicle were completed. As 10 experiments were done with methylcellulose as the vehicle there, the latest 3 of them were excluded from the present analysis to match the numbers. Therefore, each time point consists of 35 (5 rats for 7 experiments) animals.

The experimental protocols were reviewed and approved by the Ethics Review Committee for Animal Experimentation of National Institute of Health Sciences.

Microarray analysis

After collecting the blood, the animals were euthanized by exsanguination from the abdominal aorta under ether anesthesia. An aliquot of the sample (about 30 mg) for RNA analysis was obtained from the left lateral lobe of the liver in each animal immediately after sacrifice, kept in RNA later® (Ambion, Austin, TX, USA) overnight at 4 °C, and then frozen to send to the facility in the National Institute of Health Sciences.

Total RNA was isolated using RNeasy kit by Bio Robot 3000 (Qiagen, Valencia, CA, USA). Homogenization was conducted by Mill Mixer (Qiagen) and zirconium beads. Purity of the RNA was checked by gel electrophoresis confirming the 260/280 nm ratio was between 2.0 and 2.2.

Microarray analysis was conducted on 3 out of 5 samples for each group by using GeneChip® RAE230A probe arrays (Affymetrix, Santa Clara, CA, USA), containing 15923 probe sets. The procedure was conducted basically according to the manufacturer's instructions using Superscript Choice System (Invitrogen, Carlsbad, CA, USA) and T7-$(dT)_{24}$-oligonucleotide primer (Affymetrix) for cDNA synthesis, cDNA Cleanup Module (Affymetrix) for purification, and BioArray High yield RNA Transcript Labeling Kit (Enzo Diagnostics, Farmingdale, NY, USA) for synthesis of biotin-labeled cRNA. Ten micrograms of fragmented cRNA was hybridized to a RAE230A probe array for 18 h at 45 °C at 60 rpm, after which the array was washed and stained by streptavidin-phycoerythrin using

Fluidics Station 400 (Affymetrix) and scanned by Gene Array Scanner (Affymetrix).

In the middle of the project (2004), Affymetrix released ver. 2.0 GeneChip and we switched from RAE230A to 230.2. Two out of seven experiments were performed using the new chips, and they were excluded from the present analysis in order to maintain consistency. Therefore, each time point consisted of 15 measures (3 rats for 5 experiments) in the case of gene expression analysis.

The digital image files were processed by Affymetrix Microarray Suite version 5.0 and the intensities were normalized for each chip by setting the mean intensity to 500 (per chip normalization). The results of the DNA microarray analysis are available upon request (e-mail to turushid@dwe.doshisha.ac.jp).

Statistical analysis

For conventional toxicological parameters, it is common that many unimportant changes with statistical significance are observed because of the large numbers of measurements. In the present study, more than 40 parameters were measured for 8 time points (3, 6, 9, 24 h for single and 3, 7, 14, 28 days for repeated administration). For comparison between methylcellulose and corn oil, we applied Student's t-test with Bonferroni's adjustment for each parameter, i.e., p value was multiplied by 8 and $p<0.01$ was considered to be statistically significant.

For gene expression data, it is problematic to use a standard t-test, because of too many comparisons, but it is also not good to use a too conservative adjustment, because of the small

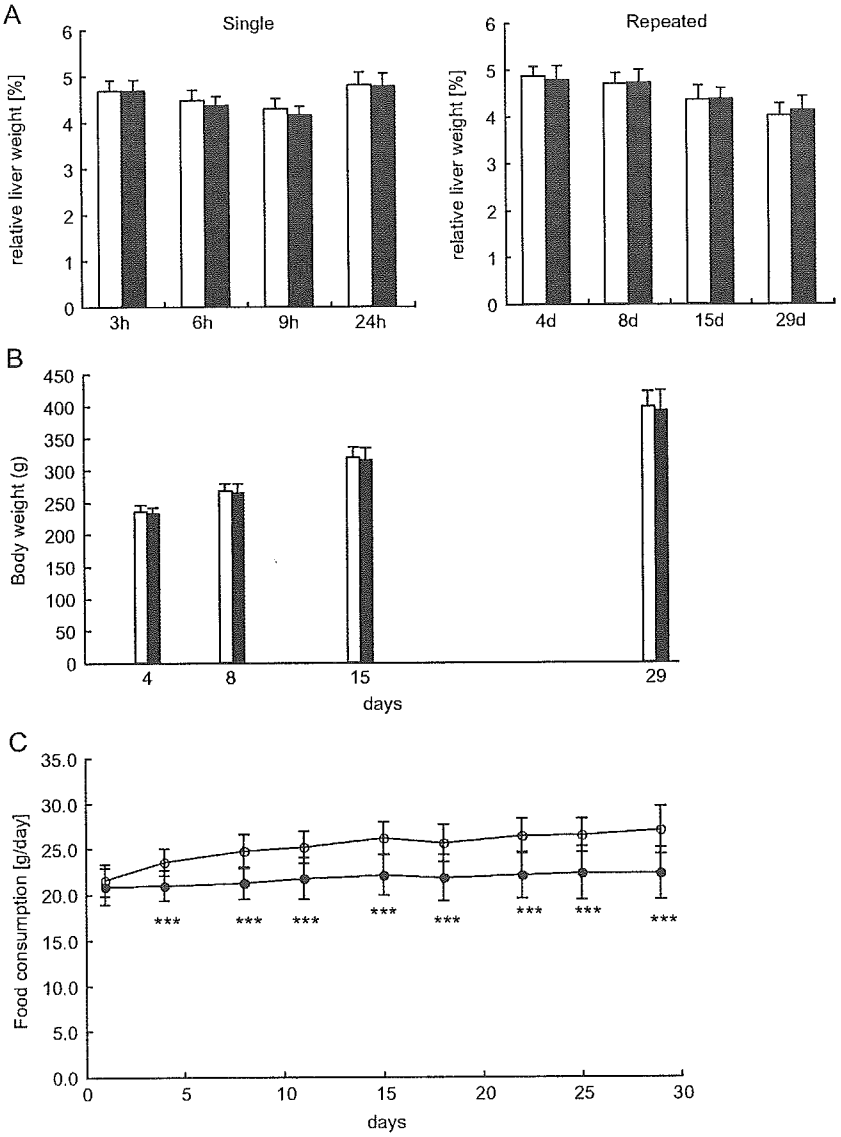

Fig. 1. Effects of different vehicles on relative liver weight, body weight, and food consumption of rats. Liver weight/body weight within 24 h after administration of vehicle and 24 h after the repeated administrations (for 3, 7, 14 and 28 days) of vehicle were measured at autopsy (A). Open and filled columns represent methylcellulose and corn oil, respectively. Body weight 24 h after the repeated administrations (for 3, 7, 14 and 28 days) of vehicle (B) and food consumption measured every 4 days and expressed as g/day (C) are plotted. Again, open and filled symbols represent methylcellulose and corn oil, respectively. Values are expressed as mean ± SD of 35 rats each for each time point. Food consumption data were obtained from rats that received either vehicle for 28 days. ***Statistically significant between methylcellulose and corn oil by Student's t-test with Bonferroni's adjustment, at $p<0.001$.

numbers of samples compared with the numbers of genes. In the present study, we considered that the β-error should be small, since our purpose was to pick up the possible vehicle effects on gene expression. Before comparison, the genes that showed less than 20 of the expression value after per chip normalization in all the samples were excluded. Genes extracted were those showing at least 1.5 fold difference between two vehicles, with $p<0.01$ (uncorrected t-test).

Results

It is common that some statistically significant but unimportant differences are observed in toxicological tests where huge numbers of parameters are measured and compared. In the present analysis of the vehicle effect, there appeared to be some differences that could not be ignored. Fig. 1A depicts the relative weight of the liver (liver weight/body weight). As is widely known, this parameter showed a clear circadian rhythm, i.e., it decreases toward the evening (9 h after dosing) and goes back in the next morning (Fig. 1A, left). In the case of rats receiving corn oil, this parameter tended to be lower than that in methylcellulose group at 6 and 9 h after dosing ($p=0.03$ and $p=0.005$, respectively, by standard t-test, but $p=0.24$ and $p=0.04$, respectively, by Bonferroni's adjustment and not significant at $p<0.01$), whereas the values returned to the same level at 24 h after administration. There was no difference in this parameter in the repeated administration, suggesting that the tendency of the decrease in the liver weight by corn oil was not accumulated during repeated dosing (Fig. 1A, right). Fig. 1 shows the body weight change (B)

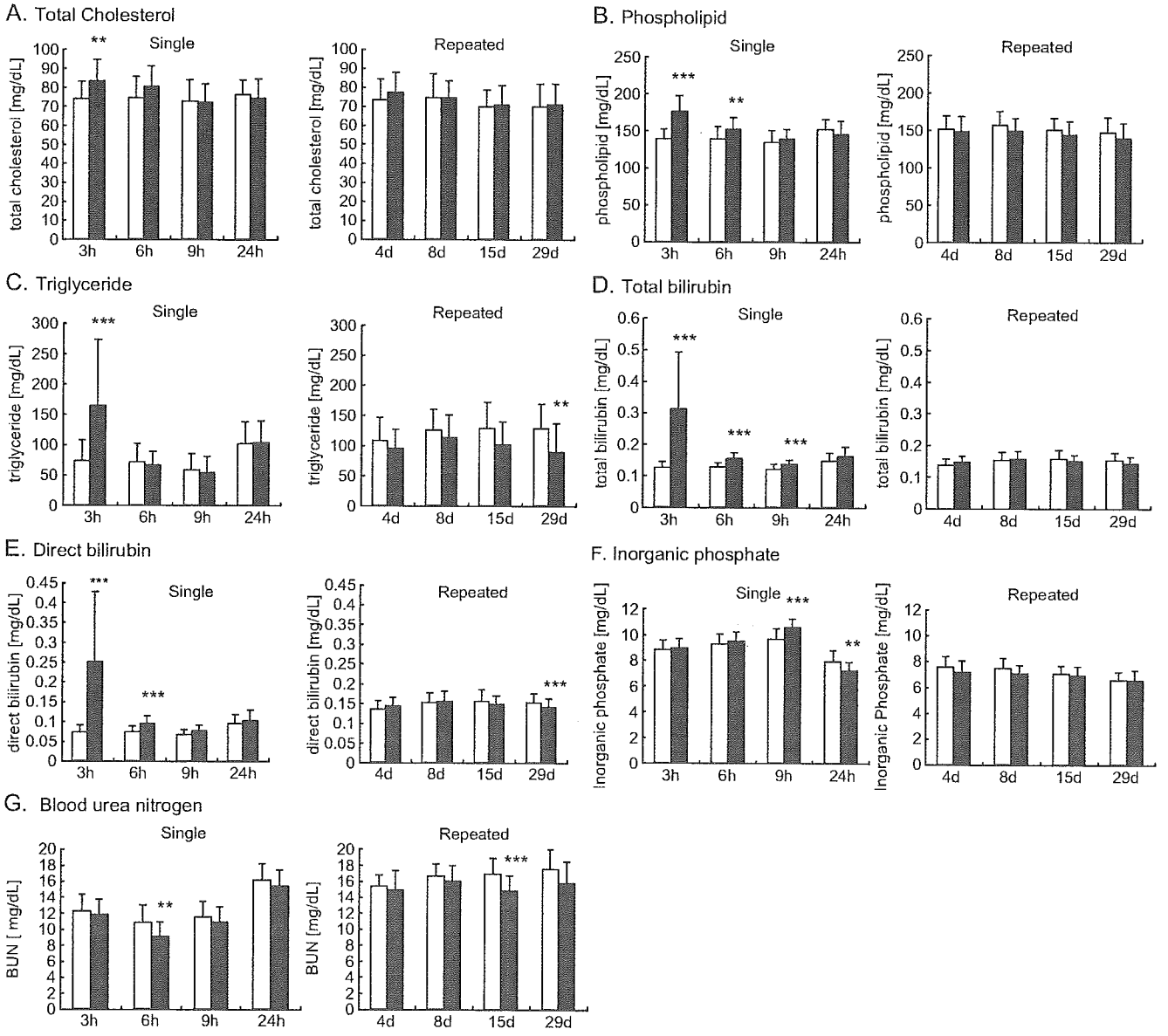

Fig. 2. Blood biochemical parameters in rats receiving methylcellulose or corn oil. Total cholesterol (A), triglyceride (B), phospholipid (C), total bilirubin (D) and direct bilirubin (E), inorganic phosphate (F), and blood urea nitrogen (G) showed a significant difference between methylcellulose (open columns) and corn oil (closed columns) among 36 parameters. Values are expressed as mean ± SD of 35 rats for each time point. Statistically significant between methylcellulose and corn oil by Student's t-test with Bonferroni's adjustment, at $^{**}p<0.01$, $^{***}p<0.001$.

Table 1
List of genes showing at least a 1.5 fold difference with $p<0.01$ (uncorrected t-test) between methylcellulose and corn oil at any point during 24 h after single dose or at 29th day of repeated dose

Probe set ID	Gene title	Gene symbol	3 h	6 h	9 h	24 h	29 d
1367707_at	fatty acid synthase	Fasn	0.995	1.738	1.300	0.722	0.596
1367708_a_at	fatty acid synthase	Fasn	0.982	1.500	1.182	0.826	0.678
1367729_at	ornithine aminotransferase	Oat	1.223	1.140	1.066	0.792	0.653
1367836_at	carnitine palmitoyltransferase 1, liver	Cpt1a	1.325	1.483	1.535	0.888	1.305
1367854_at	ATP citrate lyase	Acly	1.081	1.741	1.295	0.882	0.760
1367946_at	PDZ and LIM domain 1 (elfin)	Pdlim1	0.762	0.661	0.777	0.914	0.977
1367959_a_at	sodium channel, voltage-gated, type I, beta polypeptide	Scn1b	1.042	1.013	1.567	1.613	1.278
1368035_a_at	protein tyrosine phosphatase, receptor type, F	Ptprf	0.935	1.009	0.649	0.920	0.985
1368160_at	insulin-like growth factor binding protein 1	Igfbp1	1.239	0.485	1.238	0.631	1.143
1368272_at	glutamate oxaloacetate transaminase 1	Got1	1.623	0.989	0.965	0.687	0.813
1368275_at	sterol-C4-methyl oxidase-like	Sc4mol	0.902	1.224	1.552	0.929	0.857
1368428_at	X-prolyl aminopeptidase (aminopeptidase P) 2, membrane-bound	Xpnpep2	0.839	0.896	0.668	0.783	0.916
1368435_at	cytochrome P450, family 8, subfamily b, polypeptide 1	Cyp8b1	1.534	1.860	1.570	0.711	0.798
1368458_at	cytochrome P450, family 7, subfamily a, polypeptide 1	Cyp7a1	0.471	1.768	1.310	0.586	0.607
1368569_at	aldo-keto reductase family 1, member B7	Akr1b7	0.197	0.971	0.190	2.782	5.398
1369073_at	nuclear receptor subfamily 1, group H, member	Nr1h4	1.165	1.594	1.190	0.903	1.047
1369195_at	fatty acid binding protein 2, intestinal	Fabp2	0.901	1.135	1.022	1.753	1.753
1369238_at	inhibin beta E	Inhbe	1.441	1.553	1.067	1.034	0.934
1369415_at	basic helix-loop-helix domain containing, class B2	Bhlhb2	1.019	1.814	1.449	0.983	0.862
1369440_at	ATP-binding cassette, sub-family G (WHITE), member 8	Abcg8	0.676	0.536	0.701	0.893	1.440
1369493_at	prolactin receptor	Prlr	0.609	0.958	0.717	1.147	1.975
1369663_at	epoxide hydrolase 2, cytoplasmic	Ephx2	1.073	1.346	1.616	1.196	1.844
1369674_at	purinergic receptor P2X, ligand-gated ion channel, 5	P2rx5	1.930	0.838	0.893	0.811	1.065
1369790_at	tyrosine aminotransferase	Tat	0.771	0.624	1.094	0.735	0.837
1369864_a_at	serine dehydratase	Sds	1.509	0.429	0.872	0.482	0.538
1370024_at	Fatty acid binding protein 7, brain	Fabp7	1.044	0.964	1.057	1.312	1.524
1370336_at	pregnancy-induced growth inhibitor	Okl38	0.615	0.694	0.735	1.091	1.139
1370355_at	stearoyl-Coenzyme A desaturase 1	Scd1	1.206	1.197	1.065	0.904	0.604
1370427_at	platelet derived growth factor, alpha	Pdgfa	1.066	0.912	1.155	0.559	1.097
1371127_at	bone morphogenetic protein 1 (procollagen C-proetinase)	RGD:620739	0.815	1.175	0.950	0.991	1.557
1371234_at	fibrinogen, B beta polypeptide	Fgb	1.165	0.990	0.896	0.894	0.639
1371279_at	histone 2a /// similar to Histone H2A.1	RGD:621437	1.093	0.910	0.798	0.604	0.843
1371595_at	Transcribed locus, weakly similar to XP346694.1 Rattus norvegicus LOC360381 gene	---	0.738	0.639	0.607	0.824	0.938
1371754_at	solute carrier family 25 (mitochondrial carrier, phosphate carrier), member 25	Slc25a25	0.939	0.891	1.187	0.912	0.660
1372188_at	Endothelial cell growth factor 1 (platelet-derived) (predicted)	---	1.043	1.548	1.053	1.187	1.051
1372276_at	Transcribed locus	---	0.941	1.673	1.209	1.340	1.714
1372536_at	Chaperone, ABC1 activity of bc1 complex like (S. pombe) (predicted)	---	0.953	0.973	0.659	0.904	1.082
1374265_at	Similar to arylacetamide deacetylase (esterase) (predicted)	---	0.964	1.221	1.511	0.872	0.853
1374932_at	---	---	0.818	1.705	0.745	1.055	0.897
1375367_at	PDZ and LIM domain 2	Pdlim2	1.283	1.623	1.002	0.870	0.896
1375422_at	---	---	1.094	0.936	1.875	1.039	1.025
1375552_at	---	---	0.889	1.176	0.927	0.932	1.584

Data are expressed as the ratio of gene expression (methylcellulose=1) and columns with significant change are shaded ($N=15$ for each group).

together with food consumption (C). Although both methylcellulose and corn oil groups got weight in the same rate during repeated dosing, food consumption in the corn oil group was significantly lower than that in methylcellulose group by about 15% throughout the period of repeated administration.

Among the hematological and blood biochemical parameters, mean corpuscular hemoglobin concentration (at 15th day), platelets (at 9 h), monocytes (at 3 h), prothrombin time (at 29th day), activated partial thromboplastin time (at 24 h), fibrinogen (at 3 h), chloride (at 3 h) showed statistically significant differences between corn oil and methylcellurose. However, these changes were not considered to be important, since their changes were small and no changes in related parameters were associated. On the other hand, total cholesterol, phospholipids, triglyceride, and bilirubin (both total and direct) were found to be significantly different between vehicle controls (Fig. 2A–E). All of them showed significantly higher values in the corn oil group at 3 h after dosing, and the differences abated or disappeared at 6 h or later. In the repeated administration, the corn oil group showed rather lower values of triglyceride, total and direct bilirubin. Inorganic phosphate showed a significantly higher value in corn oil at 9 h and went down to a lower value than methylcellulose (Fig. 2F). Blood urea nitrogen (Fig. 2G) showed a lower value in corn oil at 6 h and 15th day.

Scatter plots of gene expression between vehicle controls at each time point revealed that most of the genes distributed within a 2-fold range of their 45° line, meaning that few

Table 1 (*continued*)

Probe set ID	Gene title	Gene symbol	3 h	6 h	9 h	24 h	29 d
1375619_at	---	---	1.171	0.667	0.789	0.971	0.756
1375796_at	interferon gamma induced GTPase (predicted)	Igtp_predicted	1.005	0.883	1.021	1.787	0.847
1376313_at	two pore segment channel 2 (predicted)	RGD:1311779	1.040	0.800	0.871	0.991	1.956
1376657_at	immunoglobulin superfamily, member 4A (predicted)	Igsf4a_predicted	1.060	1.749	1.510	0.868	1.022
1376704_a_at	necdin-like 2 (predicted)	Ndnl2_predicted	1.048	0.886	1.061	0.995	0.660
1376892_at	---	---	1.109	0.949	0.854	0.654	0.953
1376958_at	Similar to serine (or cysteine) proteinase inhibitor, clade B, member 9	---	0.456	0.824	1.105	1.206	1.039
1377361_at	---	---	1.004	0.667	0.794	0.890	1.020
1379252_at	Immunoglobulin superfamily, member 4A (predicted)	---	1.083	1.505	1.476	0.861	0.970
1383075_at	cyclin D1	Ccnd1	0.636	0.693	0.945	1.029	1.211
1384178_at	Leucine rich repeat containing 4B (predicted)	---	0.906	0.656	0.890	0.802	0.884
1384288_at	Transcribed locus	---	1.119	0.596	1.136	0.835	1.054
1386041_a_at	Kruppel-like factor	Klf2	1.986	0.850	1.345	1.004	1.053
1386789_at	---	---	1.305	0.611	1.196	1.134	1.003
1387017_at	squalene epoxidase	Sqle	0.927	1.279	1.832	1.058	0.980
1387022_at	aldehyde dehydrogenase family 1, member A1	Aldh1a1	0.769	1.099	0.913	1.039	1.804
1387123_at	cytochrome P450, family 17, subfamily a, polypeptide 1	Cyp17a1	1.003	0.982	1.106	1.309	1.613
1387183_at	carnitine O-octanoyltransferase	Crot	1.058	1.116	1.142	0.914	1.569
1387283_at	myxovirus (influenza virus) resistance 2	Mx2	0.721	0.777	0.503	1.565	1.280
1387307_at	histidine ammonia lyase	Hal	0.903	0.826	0.665	0.819	1.072
1387312_a_at	glucokinase	Gck	1.180	1.610	0.865	0.941	1.077
1387391_at	cyclin-dependent kinase inhibitor 1A	Cdkn1a	1.576	1.373	0.734	0.684	0.892
1387396_at	hepcidin antimicrobial peptide	Hamp	0.731	0.642	1.232	1.145	1.051
1387643_at	fibroblast growth factor 21	Fgf21	1.385	1.919	1.138	1.191	1.157
1387665_at	betaine-homocysteine methyltransferase	Bhmt	1.234	1.064	1.083	0.655	0.850
1387670_at	glycerol-3-phosphate dehydrogenase 2	Gpd2	1.169	1.650	1.430	0.872	0.864
1387730_at	paired box gene 8	Pax8	1.527	1.114	0.991	0.822	0.827
1387809_at	mitogen-activated protein kinase kinase 6	Map2k6	1.017	1.443	1.139	0.622	0.742
1387848_at	3-hydroxy-3-methylglutaryl-Coenzyme A reductase	Hmgcr	0.810	1.306	1.963	1.057	0.876
1388210_at	mitochondrial acyl-CoA thioesterase 1	Mte1	1.085	1.245	1.928	1.099	1.120
1388395_at	G0/G1 switch gene 2 (predicted)	G0s2_predicted	2.129	1.930	1.041	1.204	1.036
1388426_at	sterol regulatory element binding factor 1	Srebf1	0.648	0.787	0.694	0.855	0.885
1388531_at	progesterone receptor membrane component 2 (predicted)	Pgrmc2 predicted	1.032	1.518	1.149	0.938	1.036
1388679_at	TBC1 domain family, member 14 (predicted)	Tbc1d14 predicted	0.815	1.582	1.111	0.883	1.038
1388792_at	growth arrest and DNA-damage-inducible 45 gamma (predicted)	Gadd45 gpredicted	0.340	1.095	0.994	0.669	0.595
1388872_at	Isopentenyl-diphosphate delta isomerase	Idi1	1.029	1.077	1.772	1.249	0.870
1388924_at	angiopoietin-like protein 4	Angptl4	2.172	1.589	1.105	0.673	0.990
1389161_at	Transcribed locus	---	1.547	1.566	1.153	0.819	1.014
1389253_at	vanin 1 (predicted)	Vnn1 predicted	1.127	1.614	1.846	1.232	1.650
1389430_at	Transcribed locus	---	0.917	1.198	1.517	0.863	1.008
1390383_at	adipose differentiation-related protein	ADRP	1.296	1.784	0.870	0.952	0.913
1390607_at	nNOS-intereacting DHHC-containing Dem protein-L	RGD:1303254	0.936	1.463	1.509	0.691	0.878
1390662_at	Ab2-427	---	0.594	0.996	0.819	1.114	0.980
1392607_at	Transcribed locus	---	0.756	0.855	0.725	0.441	1.298

genes were affected by the vehicle (data not shown). Table 1 shows the list of genes that showed at least a 1.5-fold difference between vehicles with $p<0.01$ either in single dose experiment or in the 29th day of repeated dosing. Many of the genes listed are related to lipid metabolism. They were usually up-regulated by corn oil between 3 and 9 h after dosing and returned to the same level or lower at 24 h and at the 29th day. However, there were some exceptional cases, such as aldo-keto reductase 1B7 (down-regulated at 3 and 9 h but up-regulated at 24 h and 29th day), or aldehyde dehydrogenase 1A1 (only up-regulated after repeated administration). Among the genes in Table 1, there are interesting ones, i.e., CYP7A1, CYP8B1, 3-hydroxy-3-methylglutaryl-Coenzyme A reductase, fatty acid synthase, squalene epoxidase, angiopoietin-like protein 4, which are selected and shown as graphs in Fig. 3A–F. The former 5 genes all showed a circadian rhythm in that their expression in the afternoon to the evening was higher than that in the morning to noon. The administration of corn oil appeared to increase this peak. On the other hand, angiopoietin-like protein 4 showed constant expression during the day in methylcellulose, whereas corn oil markedly increased the expression of this gene at 3 and 6 h of administration.

As is obvious from Figs. 1A and 3, there exists a circadian rhythm in rat liver. In order to examine whether the observed changes were due to a disturbance in the basic rhythm, expression of various clock genes were checked and we found that the rhythm (other than that related to lipid metabolism) was relatively unaffected. As typically representative of clock genes, the expression patterns of period 2, D site albumin

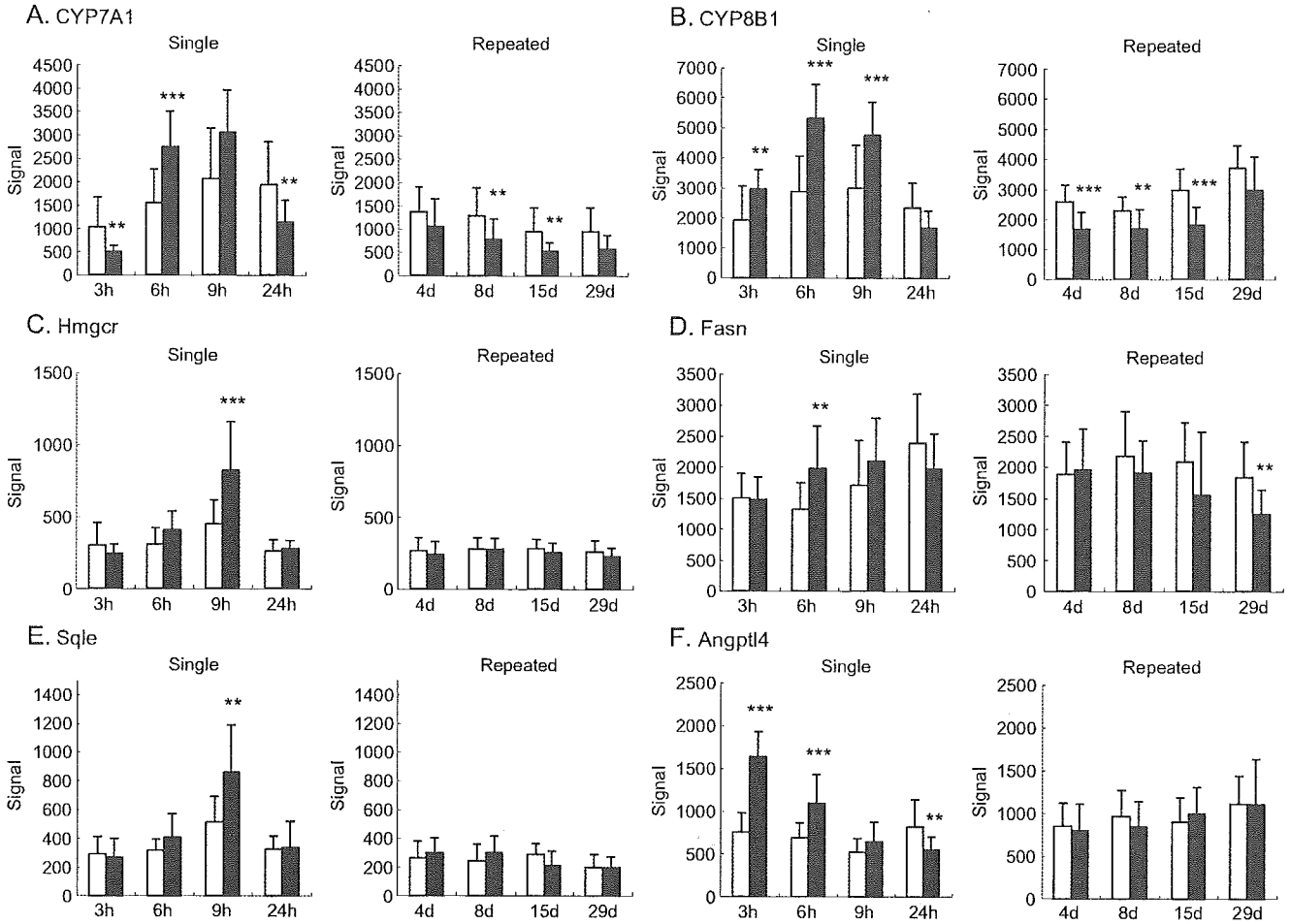

Fig. 3. Expression changes of CYP7A1 (A, Affymetrix ID 1368458_at), CYP8B1(B, Affymetrix ID 368435_at), 3-hydroxy-3-methylglutaryl-Coenzyme A reductase (C, Affymetrix ID 1387848_at), fatty acid synthase (D, Affymetrix ID 1367708_a_at), squalene opixidase (E, Affymetrix ID 1387017_at) and angiopoietin-like protein 4 (F, Affymetrix ID 1388924_at) are shown. Open and filled symbols represent methylcellulose and corn oil, respectively. Values are expressed as mean±SD of 15 rats of each for each time point. Statistically significant between methylcellulose and corn oil by uncorrected Student's *t*-test at $^{**}p<0.01$, $^{***}p<0.001$.

promoter binding protein, and arylhydrocarbon receptor nuclear translocator-like are shown in Fig. 4A–C.

Discussion

The ultimate goal of our project is to create a gene expression database for prediction of hepatotoxicity in the early stage of drug development. For this purpose, it was desirable that the vehicle for suspending drugs was unified to be methylcellulose. However, there are many test compounds with poor dispersibility, and strong detergents or organic solvents are undesirable because of their potent bioactivity, so we inevitably chose corn oil as a vehicle for the highly hydrophobic compounds.

Corn oil contains 9.2 kcal/g and supplies 10.1 kcal/day for 7-week-old rats (5 ml/kg corresponds to 1.1 g for 250 g body weight). Rats around this age consume about 25 g diet per day in the present study (Fig. 1C), which corresponds to about 90 kcal/day (CRF-1 carries 3.6 kcal/g), meaning that the administered corn oil is equal to about 11% of the total calories. Moreover, this is administered once in the morning when the feeding behavior of the rat is normally inactive. Then we were concerned that the difference between corn oil and methylcellulose cannot be ignored. In fact, the food intake of the rats in the corn oil group was significantly decreased by about 15% compared with methylcellulose group without any changes in body weight. This suggests that the rats self-controlled their total calorie intake to a constant level and so corresponding gene expression changes should have occurred.

In the acute phase, total cholesterol, triglyceride, phospholipids, and bilirubin were elevated 3 h after the administration of corn oil, which were considered to be due to rapid absorption of oil. We are not sure why plasma bilirubin was increased; it might reflect an increase in the absorption of bile components when large amounts of lipid were absorbed in the form of micelle. These parameters all returned to the same level as in the methylcellulose group 6–9 h after administration. In the repeated dose experiments, which correspond to 24 h after dosing, triglyceride and bilirubin were decreased in the corn oil group, suggesting that some adapting system lowering plasma lipid was induced during a continuous elevation of lipid component in the diet.

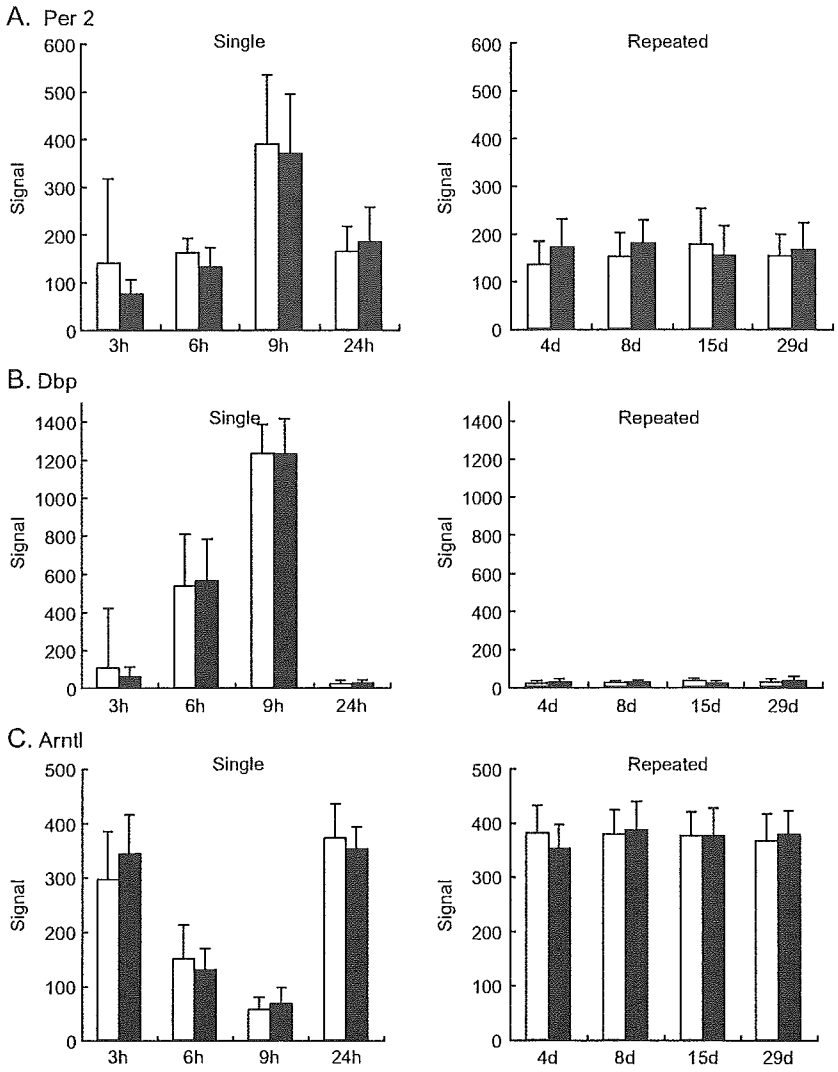

Fig. 4. Expression patterns of representative clock genes, period 2 (A, Affymetrix ID 1368303_at), D site albumin promoter binding protein (B, Affymetrix ID 1387874_at), and arylhydrocarbon receptor nuclear translocator-like (C, Affymetrix ID 1370510_a_at) are shown. Open and filled symbols represent methylcellulose and corn oil, respectively. Values are expressed as mean±SD of 15 rats for each time point. No statistically significant difference was observed between methylcellulose and corn oil at any time point.

The change in gene expression in the liver was more complex. Although the numbers of differentially expressed genes were small in respect of the total 16,000 probe sets, there were still considerable numbers of genes showing different patterns between vehicles, most of which were related to lipid metabolism. In the corn oil-treated group, the expression of CYP7A1 (cholesterol 7α hydroxylase), the rate-limiting enzyme of bile acid synthesis or elimination of cholesterol (Mast et al., 2005), showed a clear circadian rhythm as reported (Kai et al., 1995; Ishida et al., 2000), and it was lower at 3 h but higher at 6 and 9 h than that in the methylcellulose group. The expression was then lowered again at 24 h after dosing, and this pattern appeared to continue during repeated administration, i.e., the expression value in the corn oil group stayed about 60% of those in the methylcellulose group until the 29th day. On the other hand, CYP 8B1 (cholesterol 12α hydroxylase), which catalyzes the synthesis of cholic acid and controls the ratio of cholic acid over chenodeoxycholic acid in the bile, showed a less marked but obvious circadian pattern as reported (Ishida et al., 2000). It showed a continuously higher expression from 3 to 9 h than methylcellulose, returned to the same level at 24 h, and no difference was observed in the repeated dosing. These changes were considered to be the reflection of the transiently high consumption of bile due to the bolus injection of corn oil.

The rate-limiting enzyme of cholesterol biosynthesis, 3-hydroxy-3-methylglutaryl-Coenzyme A reductase, also showed a circadian rhythm and the administration of corn oil markedly increased its expression at 9 h. At this point, squalene epoxidase and sterol-C4-methyloxidase were also increased. The former is a microsomal enzyme that catalyzes the oxidation of squalene to 2,3-oxidosqualene, the last reaction of non-sterol metabolites in the cholesterol biosynthesis pathway (Hidaka et al., 1990). The latter is known as one of the components essential for sterol biosynthesis in yeast (Darnet and Rahier, 2003), and it used to be termed neurorepl and was discussed in relation to the repair

process of damaged neurons (Uwabe et al., 1997). Looking at the high expression level in liver and induction by corn oil alone, we considered that the induction of sterol-C4-methyloxidase was a general phenomenon related to lipid metabolism rather than neurophysiology.

One noticeable gene is angiopoietin-like protein 4, which was recently shown to be involved not only in lipid metabolism via inhibition of lipoprotein lipase activity (Yoshida et al., 2002) but also in various diseases (Xu et al., 2005). It was reported that its expression in adipose tissue and liver was affected by the nutrient status, e.g., induced by fasting (Ge et al., 2005). In the present study, this gene was markedly up-regulated at 3–6 h after corn oil treatment and returned to the same level as methylcellulose at 9 h or later. It is of interest to elucidate why oil intake resembles fasting in case of angiopoietin-like protein 4 expression.

Fatty acid synthase was up-regulated by corn oil at 6 h after dosing and then returned to the same level as methylcellulose, whereas it was down-regulated (about 60% of methylcellulose) after repeated administration. In contrast, fatty acid binding protein family members, involved in lipid uptake, were up-regulated 24 h after single and repeated administrations of corn oil. These reactions in the repeated phase are considered to be adaptive responses suitable for lipid intake. In addition to these two enzymes, there were genes showing significantly different expression in the corn oil group at 29th day, i.e., serine dehydratase, ornithine aminotransferase, stearoyl CoA desaturase, aldehyde dehydrogenase 1A1, and epoxide hydroxylase 2. Of these, the latter two were up-regulated whereas the others were down-regulated.

The increase of aldehyde dehydrogenase and epoxide hydroxylase is considered to be favorable for the condition of high lipid diet, since both enzymes are reported to be involved in the detoxication of the metabolites associated with lipid metabolism (Choudhary et al., 2005; Newman et al., 2005). As for the down-regulated genes, the decrease of fatty acid synthase and stearoyl CoA desaturase, both are in the pathway of fatty acid synthesis, which might reflect a decrease in the need of fatty acid. Serine dehydratase and ornithine aminotransferase are known to be induced by high protein diet, glucagon, or glucocorticoid (Hunter and Harper, 1977; Bourdel et al., 1983). Based on the present data, it is difficult to conclude whether the change was due to the relative reduction of protein in the diet, or to the secondary change in endocrinological status. Moreover, it should be noted that the circadian pattern could not be obtained in the present experiments of repeated administration. Although most of the observed changes could be interpreted as an adaptation for the rapid absorption of oil from the gut in the acute phase and for the continuously elevated composition of lipid in the food in the chronic phase, it is difficult to map all the changes to various metabolic pathways, and to give reasonable explanations. Further confirmation is obviously needed, but the present study has supplied many valuable suggestions.

Many of the genes affected by corn oil treatment exhibit their own circadian rhythm generally with low expression at 3 h (around noon), increasing from 6 h (late afternoon) to 9 h (evening), and returning to low expression at 24 h (morning) of dosing. There is a long blank period between 9 and 24 h after dosing, as it was practically impossible to perform measurements after midnight in the present project. It was therefore possible that the actual peak of some genes occurred between 9 and 24 h after dosing, or midnight. We were concerned that the compulsory administration of oil in the morning disturbs not only feeding behavior but also the circadian rhythm itself. However, it was confirmed that the expression patterns of representative clock genes were unaffected, suggesting that changes in gene expression were not due to the disturbance of the original circadian rhythm. Moreover, the expression levels of clock genes in repeated dosing (corresponding to the 24 h value) were also unchanged, suggesting that disturbance of the circadian rhythm during repeated administration of oil was unlikely.

The present analysis of the data in our database would provide useful information for future experiments to elucidate the detailed mechanism of lipid metabolism. It also provides valuable information for the analysis of the activity of compounds when a comparison of chemicals dosed with different vehicles is made. Since the data accumulated in our database appeared to be of high quality and reproducibility, at least in terms of the effect of vehicles, we expect that drug actions, especially related to toxicity, may be sensitively detected using our database.

Acknowledgements

This study was supported in part by a grant from the Ministry of Health, Labour and Welfare (H14-Toxico-001).

References

Bourdel, G., Hitier, Y., Lardeux, B., Girard-Globa, A., 1983. Activity of several enzymes of amino acid catabolism in the liver of rats fed protein as a meal. Reproduction Nutrition Development 23, 875–881.

Choudhary, S., Xiao, T., Srivastava, S., Zhang, W., Chan, L.L., Vergara, L.A., Van Kuijk, F.J., Ansari, N.H., 2005. Toxicity and detoxification of lipid-derived aldehydes in cultured retinal pigmented epithelial cells. Toxicology and Applied Pharmacology 204, 122–134.

Darnet, S., Rahier, A., 2003. Enzymological properties of sterol-C4-methyl-oxidase of yeast sterol biosynthesis. Biochimica et Biophysica Acta 1633, 106–117.

Ge, H., Cha, J.Y., Gopal, H., Harp, C., Yu, X., Repa, J.J., Li, C., 2005. Differential regulation and properties of angiopoietin-like proteins 3 and 4. Journal of Lipid Research 46, 1484–1490.

Hidaka, Y., Satoh, T., Kamei, T., 1990. Regulation of squalene epoxidase in HepG2 cells. Journal of Lipid Research 31, 2087–2094.

Hunter, J.E., Harper, A.E., 1977. Induction of pyridoxal phosphate-dependent enzymes in vitamin B-6 deficient rats. Nutrition 107, 235–244.

Ishida, H., Yamashita, C., Kuruta, Y., Yoshida, Y., Noshiro, M., 2000. Insulin is a dominant suppressor of sterol 12 alpha-hydroxylase P450 (CYP8B) expression in rat liver: possible role of insulin in circadian rhythm of CYP8B. Journal of Biochemistry (Tokyo) 127, 57–64.

Kai, M.-H., Eto, T., Kondo, K., Setoguchi, Y., Higashi, S., Maeda, Y., Setoguchi, T., 1995. Synchronous circadian rhythms of mRNA levels and activities of cholesterol 7 alpha-hydroxylase in the rabbit and rat. Journal of Lipid Research 36, 367–374.

Mast, N., Graham, S.E., Andersson, U., Bjorkhem, I., Hill, C., Peterson, J., Pikuleva, I.A., 2005. Cholesterol binding to cytochrome P450 7A1, a key enzyme in bile acid biosynthesis. Biochemistry 44, 3259–3271.

Newman, J.W., Morisseau, C., Hammock, B.D., 2005. Epoxide hydrolases: their roles and interactions with lipid metabolism. Progress in Lipid Research 44, 1–51.

Urushidani, T., Nagao, T., 2005. Toxicogenomics: the Japanese initiative. In: Borlak, J. (Ed.), Handbook of Toxicogenomics—Strategies and Applications. Wiley-VCH, pp. 623–631.

Uwabe, K., Gahara, Y., Yamada, H., Miyake, T., Kitamura, T., 1997. Identification and characterization of a novel gene (neurorep 1) expressed in nerve cells and up-regulated after axotomy. Neuroscience 80, 501–509.

Waring, J.F., Ulrich, R.G., Flint, N., Morfitt, D., Kalkuhl, A., Staedtler, F., Lawton, M., Beekman, J.M., Suter, L., 2004. Interlaboratory evaluation of rat hepatic gene expression changes induced by methapyrilene. Environmental Health Perspectives 112, 439–448.

Xu, A., Lam, M.C., Chan, K.W., Wang, Y., Zhang, J., Hoo, R.L., Xu, J.Y., Chen, B., Chow, W.S., Tso, A.W., Lam, K.S., 2005. Angiopoietin-like protein 4 decreases blood glucose and improves glucose tolerance but induces hyperlipidemia and hepatic steatosis in mice. Proceedings of the National Academy of Sciences of the United States of America 102, 6086–6091.

Yoshida, K., Shimizugawa, T., Ono, M., Furukawa, H., 2002. Angiopoietin-like protein 4 is a potent hyperlipidemia-inducing factor in mice and inhibitor of lipoprotein lipase. Journal of Lipid Research 43, 1770–1772.

Available online at www.sciencedirect.com
SCIENCE DIRECT®
Experimental Neurology 198 (2006) 154–166
Experimental Neurology
www.elsevier.com/locate/yexnr

Cell cycle and cell death regulation of neural progenitor cells in the 5-azacytidine (5AzC)-treated developing fetal brain

Masaki Ueno*, Kei-ichi Katayama, Hirofumi Yamauchi, Hiroyuki Nakayama, Kunio Doi

Department of Veterinary Pathology, Graduate School of Agricultural and Life Sciences, The University of Tokyo, 1-1-1 Yayoi, Bunkyo-ku, Tokyo 113-8657, Japan

Received 28 April 2005; revised 22 November 2005; accepted 22 November 2005
Available online 19 January 2006

Abstract

In the developing brain, neural progenitor cells are susceptible to many extrinsic stresses, including DNA damage. We treated pregnant rats with 5-azacytidine (5AzC), a DNA demethylating and damaging agent, to investigate the cellular responses of the fetal brain, focusing on the regulation of proliferation and cell death. 5AzC first induced the accumulation of cells in abnormal mitosis, G2-phase accumulation, and then apoptosis of the neural progenitor cells. Most of the apoptotic cells were in G1 phase. Cell cycle transition studies suggested that G2/M progression was blocked, after which the cells moved to G1 phase or underwent apoptosis. p53, a key factor for response to DNA damage, and some of its target genes showed increased expression in Western blot and DNA microarray analyses. In 5AzC-treated fetal brains of p53-deficient mice, apoptosis did not occur, although G2/M accumulation was induced. These results suggest that, in the developing brain, apoptosis is p53-dependent but that another mechanism governs the G2/M checkpoint. The G2/M regulator, Cdc2, was activated by dephosphorylation through G2/M accumulation, suggesting accelerated entry into mitosis leading to accumulation of cells showing abnormal mitosis. Furthermore, some cells may have died due to mitotic catastrophe. Throughout brain development, various cell cycle and cell death regulation mechanisms provide neural progenitor cells with options for defense from DNA damage.

Keywords: Apoptosis; 5-azacytidine; Cell cycle arrest; DNA damage; Interkinetic nuclear migration; Mitotic catastrophe; Neural progenitor cell; p53; Ventricular zone

Introduction

Environmental stresses and stimuli can induce deleterious effects on brain development. The fetal central nervous system (CNS) is sensitive to diverse environmental factors because a large number of processes occur during an extended period of development, and fetal neural damage is an important issue affecting the completion of normal CNS development (Rodier, 1995; Mendola et al., 2002; Costa et al., 2004).

In the developing brain, multipotent neural progenitor cells proliferate in the ventricular zone (VZ), after which they differentiate into neural cells, i.e., neurons, astrocytes, and oligodendrocytes (Rao, 1999; Qian et al., 2000; Temple, 2001). In the early developmental stage, they form a pseudostratified epithelium in the VZ, so they also are called neuroepithelial cells. The nuclei of proliferating neural progenitor cells undergo a characteristic migration–interkinetic nuclear migration (or "elevator movement")–in the VZ, in which the positions of nuclei are correlated with their cell cycle phase (Takahashi et al., 1995; Fujita, 2003). In brief, the S phase nuclei located in the outer area of the VZ translocate inward during G2 phase, and mitosis occurs at the ventricular surface. Then, the nuclei migrate outward during G1 and enter S phase again (Fig. 7A). In this way, neural progenitor cells proliferate.

The balance between proliferation and cell death (apoptosis) is important for correct development of the brain (Oppenheim, 1991; Blaschke et al., 1996; Thomaidou et al., 1997). Moreover, the regulation of this balance also seems to be important during damage due to extrinsic stresses, particularly that from anti-proliferative stimuli. However, it remains unclear how neural progenitor cells in the fetal brain react toward extrinsic stresses, especially regarding the regulation of proliferation and cell death, while the organ is still developing.

5-Azacytidine (5AzC) is an agent that has two characteristic effects that interfere with the brain development, i.e. disturbance

* Corresponding author. Fax: +81 3 5841 8185.
E-mail address: ms-ueno@umin.ac.jp (M. Ueno).

0014-4886/$ – see front matter © 2005 Elsevier Inc. All rights reserved.
doi:10.1016/j.expneurol.2005.11.024

of DNA methylation and DNA damage. During the development of the CNS as well as other organ systems, DNA methylation is a key step for regulating gene expression (Sun et al., 2003), and agents such as 5AzC may disturb gene expression, and subsequently organogenesis, through their DNA demethylating effects. 5AzC also is thought to act as a DNA damaging agent (Juttermann et al., 1994; Karpf et al., 2001), and DNA damage causes serious abnormalities in the developing brain (Gao et al., 1998; Vinson and Hales, 2002; D'Sa et al., 2003). In our previous study, we demonstrated that 5AzC treatment of the pregnant rats prompted neural progenitor cells in the fetal brain to undergo apoptotic cell death; the treatment also led to delayed migration of nuclei, suggesting that cell cycle arrest might occur (Ueno et al., 2002a,b). In addition, our data indicated that these events might be dependent on p53, a tumor suppressor protein, and its transcriptional target genes such as $p21^{waf1/cip1}$. p53 is known to play a key role in the induction of cell growth arrest and apoptosis in response to DNA damage (May and May, 1999; Lakin and Jackson, 1999). However, despite these observations, it was unclear at which cell cycle phase the neural progenitor cells arrested and underwent apoptosis due to 5AzC treatment.

In the present study, we exposed fetal rat brains to 5AzC to examine how the neural progenitor cells response to extrinsic stresses, focusing on the regulation of apoptosis and cell cycle kinetics. We used flow cytometric methods for investigating alterations in cell cycle distribution and assessing the cell cycle position of apoptotic cells. Furthermore, we evaluated alteration of gene expression by using DNA microarray technology to reveal various mechanisms underlying cellular responses to 5AzC. In our examination, we focused on the role of p53 in the regulation of apoptosis and the cell cycle, and we used p53-knockout mice to confirm these points. We found that both p53-dependent and -independent mechanisms were involved in the regulation of apoptosis and the cell cycle of 5AzC-treated neural progenitor cells.

Materials and methods

All procedures were approved by the Animal Care and Use Committee of the Graduate School of Agricultural and Life Sciences, The University of Tokyo.

Animals

Pregnant Jcl:Wistar rats were obtained from Japan CLEA (Tokyo, Japan). $p53^{+/-}$ mice (C57BL/6 TSG-p53 N5 Targeted Mutation) were purchased from Taconic (Germantown, NY). Heterozygous mice were crossed to generate wild-type, heterozygous, and homozygous gene-disrupted mice. Endogenous and disrupted genes were detected by polymerase chain reaction analysis of tail DNA extracts, as described by Timme and Thompson (1994).

Chemicals

5AzC and 5-bromo-2′-deoxyuridine (BrdU) were obtained from Sigma (St. Louis, MO).

Treatments for Wistar rats

On day 13 of gestation pregnant, rats were injected intraperitoneally (i.p.) with 10 mg/kg of 5AzC and then euthanized at 1, 3, 6, 9, and 12 h after treatment. The dose was selected according to that of a previous study, in which 10 mg/kg of 5AzC caused high induction of neural cell apoptosis and low fetal mortality (Lu et al., 1998). As controls, pregnant rats were injected with an equivalent volume of saline and euthanized at 1, 3, 6, 9, and 12 h after treatment. Collected fetuses underwent histopathological examination, and cell cycle, DNA microarray, and Western blot analyses.

Treatments for p53-knockout mice

Pregnant mice were injected i.p. with 10 mg/kg of 5AzC on day 12 of gestation and euthanized at 6 and 12 h after treatment. As controls, dams were injected i.p. with an equivalent volume of saline on day 12 of gestation and were euthanized at 6 h after treatment. Collected fetuses were subjected to histopathological examination and cell cycle analysis.

Histopathological examination and immunohistochemistry

Collected fetuses were fixed in 10% neutral-buffered formalin and embedded in paraffin. Paraffin sections (thickness, 4 μm) were stained with hematoxylin and eosin for histopathological examination. The dorsal telencephalic wall was mainly examined.

Some of the sections underwent immunohistochemical staining for cleaved caspase-3 and phospho-histone H3 by the LSAB method with streptavidin (Dako, Carpinteria, CA). Rabbit anti-cleaved caspase-3 polyclonal antibody (Cell Signaling Technology, Beverly, MA) and rabbit anti-phospho-histone H3 polyclonal antibody (Cell Signaling Technology) were used as the primary antibodies and biotin-labeled goat anti-rabbit IgG (Kirkegaard and Perry, Gaitherburg, MD) as the secondary antibody.

Staining for p53 and $p21^{waf1/cip1}$ was performed with an Envision+ Kit (Dako), as previously reported (Ueno et al., 2002a). Rabbit anti-p53 polyclonal antibody (Santa Cruz Biotechnology, Santa Cruz, CA) and mouse anti-p21 monoclonal antibody (Pharmingen, San Diego, CA) were used as the primary antibodies. The positive signals were visualized using a peroxidase-diaminobenzidine reaction, and then the sections were counterstained with methyl green.

Cell cycle analysis

Telencephalons of two or three fetuses from each dam (1 to 12 h after treatment, and controls) were obtained carefully under stereoscopic microscopy and then prepared for flow cytometric analysis. The cells isolated from the telencephalons from each dam were resuspended in HBSS. The concentration of the resuspended cells was adjusted to $1–2 \times 10^6$. They were centrifuged for 5 min at $1500 \times g$ at 4°C, and the supernatant was discarded. After being washed in Dulbecco's PBS (dPBS), the cells were fixed in 70% ethanol at 4°C overnight. Cells then

were washed in dPBS and incubated with ribonuclease A (RNase A; 250 μg/ml, Sigma) for 40 min at 37°C. Cells were stained with propidium iodide (PI; 50 μg/ml, Sigma) for 30 min on ice. Cell cycle analysis was performed using the FACS Callibur system (Becton Dickinson, Mountain View, CA), and cell cycle distribution was analyzed using the Cell Quest program (Becton Dickinson).

Detection of BrdU-positive cells in the cell cycle

Pregnant rats on day 13 of gestation were injected i.p. with 10 mg/kg of 5AzC and 20 mg/kg of BrdU concurrently and then euthanized at 1, 3, 6, 9, and 12 h after treatment. As controls, pregnant rats were injected only with BrdU and euthanized at 1, 3, 6, 9, and 12 h after treatment. Collected fetuses underwent flow cytometric analysis to investigate the transition of BrdU-incorporated cells in the cell cycle. Cells isolated from two or three fetal telencephalons were resuspended and then washed and fixed using the same method described for cell cycle analysis. After being fixed in 70% ethanol, the cells were washed with dPBS and then resuspended for 30 min at room temperature (RT) in 2 M HCl containing 0.5% Triton X-100. After being neutralized in 0.1 M $Na_2B_4O_7$, the cells were incubated with FITC-labeled anti-BrdU monoclonal antibody (Pharmingen, San Diego, CA) for 30 min at RT. They then were resuspended in dPBS containing PI (10 μg/ml) for 30 min on ice and analyzed using the FACS Callibur system and Cell Quest program (Becton Dickinson).

Detection of fragmented DNA

Fragmented DNA was detected with an APO-BrdU Kit (Pharmingen). The manufacturer's protocol was followed with minor modifications. Cells were isolated from three rat fetal telencephalons from each dam (9 and 12 h after treatment, and controls) as for cell cycle analysis and first fixed in 1% paraformaldehyde in dPBS for 15 min on ice. After being washed with dPBS, they were fixed in 70% ethanol at 4°C for one or two overnights. Cells then were washed in the Wash Buffer from the kit and incubated in the DNA Labeling Solution for 60 min at 37°C. In this solution, the multiple fragmented DNA 3′-OH ends in the nuclei were labeled with Br-dUTP in the presence of terminal deoxynucleotidyl transferase (TdT). After being washed in Rinse Buffer, cells were incubated for 30 min at RT in Antibody Staining Solution containing FITC-labeled anti-BrdU antibody and then stained with PI/RNase A solution for 30 min at RT. FITC-positive apoptotic cells were detected and analyzed using the FACS Callibur system (Becton Dickinson) and Cell Quest program (Becton Dickinson).

RNA extraction and microarray analysis

Microarray expression analysis was performed using the Affymetrix GeneChip system (Santa Clara, CA) according to the manufacturer's instructions. Six to eight rat fetal telencephalons were acquired from each dam (6, 9, or 12 h after treatment, and controls, $n = 2$ dams per time point), and total RNA was extracted with the RNeasy Mini Kit (Qiagen, Germantown, MD). The quality and quantity of the extracted RNA samples were examined by agarose gel electrophoresis. Then, double-stranded cDNA was synthesized from total RNA. The first cDNA strand was prepared from 10 μg of total RNA by using SuperScript II RNase H⁻ Reverse Transcriptase (Invitrogen) and the T7-$(dT)_{24}$ primer (primer sequence, 5′-GGCCAGTGAATTGTAATACGACTCACTATAGG-GAGGCGG-$[dT]_{24}$-3′, Amersham Bioscience, Tokyo, Japan). The second strand was synthesized using the SuperScript Double-stranded cDNA Synthesis Kit (Invitrogen). Then, biotin-labeled cRNA was synthesized from the double-stranded cDNA by using the Enzo High-yield RNA Transcription Labeling Kit (Enzo Diagnostics, NY) and purified with the RNeasy Mini Kit (Qiagen). Twenty micrograms of biotin-labeled cRNA was then fragmented in a fragmentation buffer. Fragmented cRNA was mixed in a hybridization solution prepared with a GeneChip Eukaryotic Hybridization Control Kit (Affymetrix) and hybridized to the Affymetrix Rat Expression Array 230A for 16 h at 45°C while being rotated at 60 rpm in a GeneChip Hybridization Oven 640 (Affymetrix). The chips were then washed and stained automatically with a Fluidics Station (Affymetrix) and scanned with the GeneArray Scanner (Hewlett Packard, Palo Alto, CA).

Microarray data analysis

The microarray imaging data were analyzed using MicroarraySuite ver. 5.0 (Affymetrix). After hybridization intensity data were captured, the intensity values of each probe were calculated automatically. Data were compared between the treated and control groups. Prior to comparing any two measurements, scaling and normalizing procedures were performed. In the case of a pairwise comparison of two array results, the patterns of change of the whole probe set were used to make a qualitative call (called difference call) of "Increase (I)", "Decrease (D)", "Marginal increase (MI)", "Marginal decrease (MD)", or "No change (NC)", in which statistical analysis was done following the manufacturer's guide (MicroarraySuite ver 5.0 User's Guide). We then extracted the groups of genes corresponding to I, MI, D, or MD in both samples at each time point and performed pathway analyses as mentioned below. The fold change in gene expression was derived from the ratio of the average difference from one experimental array compared with a control array.

The extracted genes underwent signal pathway analysis with GenMAPP (http://www.GenMAPP.org). This analysis involves the uploading of gene expression data onto known biologic pathways and a list of genes that is categorized with gene functions. Data regarding each gene are easily visualized, including its change in expression and roles in various signal cascades.

Real-time PCR

Some of the total RNA extracted for microarray analysis was subjected to reverse transcription for the first-strand cDNA synthesis by using an oligo $(dT)_{12-18}$ primer and

SuperScript II RNase H⁻ Reverse Transcriptase (Invitrogen). Real-time PCR was performed using oligonucleotide primers sets corresponding to the cDNA sequences of *cyclin B1*, *Cdc20*, and *glyceraldehyde-3-phosphate dehydrogenase* (*GAPDH*). Sense and antisense primers were as follows: *cyclin B1*, sense 5′-CAGAGGTGGAACTGGATGAGC-3′ and antisense 5′-GGGCTTGGAGAGGGAGTATCA-3′; *Cdc20*, sense 5′-AGGAGGTACCAGTGACCGACA-3′ and antisense 5′-ACCAGAGGATGGAGCACACC-3′; and *GAPDH*, sense 5′-CCTGCACCACCAACTGCTTAG-3′ and antisense 5′-CATGGACTGTGGTCATGAGCC-3′. In brief, 25 μl of reaction mixture containing 12.5 μl SYBR Green Real-time PCR Master Mix (Toyobo, Osaka, Japan), 0.2 μM each of the sense and antisense primers, and 1 μl of the cDNA sample was preheated at 95°C for 3 min and then underwent 40 cycles of amplification (denaturation at 95°C for 15 s, annealing and extension at 60°C for 1 min) by using the ABI PRISM 7900 HT Sequence Detection System (Applied Biosystems, Foster City, CA). Relative intensity against *GAPDH* was calculated, and fold change relative to the control was represented as the mean ± standard deviation (SD) of 2 dams.

Western blotting

Four or five rat fetal telencephalons (3 to 12 h after treatment, and controls) were homogenized in a solution of 20 mM Tris–HCl (pH 7.4) containing 150 mM NaCl, 1 mM PMSF, 1% aprotinin, 2 mM EDTA, 2 mM Na_3VO_4, 1% NP-40, 0.1% SDS, and 1 mM DTT and centrifuged at 12,000 × *g* for 20 min at 4°C. Approximately 30 μg of extract was loaded per lane of a 10% SDS-PAGE gel, electrophoresed, and transferred to a PVDF membrane (Bio-Rad, Hercules, CA). Blots first were probed with antibodies to p53 (Santa Cruz), Chk2 (Santa Cruz), $p21^{waf1/cip1}$ (Pharmingen), cyclin B1 (NeoMarkers, Fremont, CA), Cdc2 (Cell Signaling Technology), phospho-Cdc2 (Tyr16) (Cell Signaling Technology), and β-actin (Sigma). After incubation with the appropriate secondary antibody conjugated to horseradish peroxidase (Amersham, Buckinghamshire, UK), detection was performed with the ECL Plus kit (Amersham).

Results

Histopathological changes

Histopathological changes induced by 5AzC-treatment were almost same in the VZ of all area of telencephalon, i.e. telencephalic wall and basal ganglia. In this study, therefore, we chose dorsal telencephalic wall to observe the changes.

We first counted mitotic cells with phospho-histone H3, a marker of mitosis. Although this antigen is also present in late G2 phase, we counted only the phospho-histone-H3-positive cells which have mitotic figures. At 6 h after 5AzC treatment, the number of mitotic cells positive for phospho-histone H3 was increased in the VZ along the ventricle (Figs. 1A and B). These

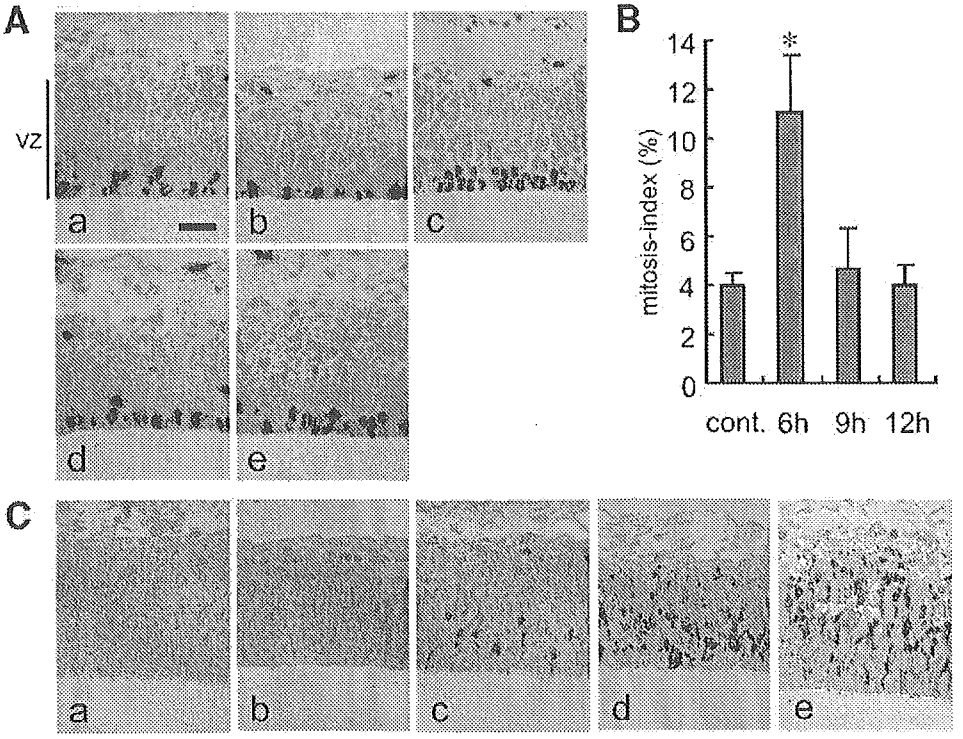

Fig. 1. Histopathological changes in the VZ of dorsal telencephalic wall of rat fetus. (A) Staining for phospho-histone H3, a mitotic marker (a: control (12 h), b: 3 h, c: 6 h, d: 9 h, and e: 12 h). Mitoses are observed mainly along the ventricular surface throughout the experimental period. Mitotic cells remarkably increased at 6 h (c). (B) The mitosis index (%) of neural progenitor cells at the ventricular surface. The indices (%; the number of phospho-histone-H3-positive cells with mitotic figures/500 cells in the VZ) are represented as the mean ± SD ($n = 3$). *$P < 0.05$; significantly different from the control (12 h) (Student's *t* test). Mitotic cells remarkably increased at 6 h and then decreased to the control level. (C) Staining for cleaved caspase-3, an apoptosis marker (a: control (12 h), b: 3 h, c: 6 h, d: 9 h, and e: 12 h). The number of cleaved caspase-3-positive cells appeared at 6 h and increased from 9 to 12 h. Scale bar: 50 μm.

results coincide with those of our previous study, in which we observed aberrant accumulation of mitotic cells with abnormal morphology along the ventricle (Ueno et al., 2002b). These cells gradually decreased in number after 6 h. From 6 to 12 h, the number of pyknotic cells, which had the morphological characteristics of apoptotic cells (Ueno et al., 2002b), increased among the neural progenitor cells in the VZ. Immunohistochemically, the pyknotic cells were stained positively for cleaved caspase-3 (Fig. 1C), which is known to be involved in neural cell apoptosis during development as well as in the apoptosis of neurons induced by DNA-damaging agents (Kuida et al., 1996; Keramaris et al., 2000).

Cell cycle analysis

In E12 to E13 mice, about 70% of cells in the fetal telencephalon are neural progenitor cells (D'Sa-Eipper and Roth, 2000), so we believe that the cells we analyzed reflected the cell cycle distribution of neural progenitor cells (Fig. 2). Furthermore, most of the neural progenitor cells that we analyzed were thought to localize in the VZ, rather than the subventricular zone (SVZ), the other area where neural progenitor cells proliferate, because the SVZ is not yet prominent in E13 rat (Fig. 1A).

The cell cycle distribution from 1 to 3 h after 5AzC treatment did not markedly differ from that of the control. At 6 h, the number of cells in G2/M phase increased (control, 8.8 ± 0.7%; 5AzC, 15.0 ± 0.9%) and that in G0/G1 decreased (control, 72.5 ± 1.4%; 5AzC, 61.6 ± 1.0%). This phenomenon likely relates to the accumulation of mitotic cells along the ventricle, as observed in the histopathological analysis (Figs. 1A-c and B). At 9 h, the number of cells in G2/M further increased (16.1 ± 0.6%), that of S phase increased slightly, and that of G0/G1 decreased. These results suggest that cell cycle progression was blocked and delayed at the S/G2 and G2/M transitions. Although phospho-histone-H3-positive cells with mitotic figures decreased at 9 h compared to 6 h (Fig. 1B), the number of cells in the G2/M phase increased at 9 h. It indicates that, at 9 h, G2 progression was blocked while the degree of mitotic accumulation decreased. Furthermore, apoptotic cells began to appear in the sub-G1 area from 6 to 9 h after 5AzC treatment. At 12 h, the number of cells accumulated in G2/M was reduced, the number of cells in the S phase decreased, and that of G0/G1 increased. At the same time, the number of apoptotic cells remarkably increased (15.8 ± 3.2%). In light of these results, the G2/M block appeared to have been released and the cells shifted to G0/G1 after mitosis, or to apoptosis.

Detection of BrdU-positive cells in the cell cycle

To confirm that cells shifted from accumulation at G2/M and either entered G0/G1 or became apoptotic, we injected BrdU (20 mg/kg) and used a flow cytometry to investigate the cell cycle transition of 5AzC-treated neural progenitor cells. 5AzC and BrdU both are incorporated into DNA during the S phase of the cell cycle.

In the BrdU-only control group, BrdU first was incorporated into S-phase cells at 1 h after treatment (Fig. 3). At 3 h, the BrdU-incorporated cells had transitioned from S to G2/M phase, and some had entered G0/G1. At 6 h, most of the BrdU-positive cells had exited S phase and were in G2/M or G0/G1. At 9 h, some BrdU-positive cells had re-entered S phase, and most of them had returned to S phase by 12 h. The duration of a single complete cell cycle is thought to be at least 12 h, an assumption that is supported by the previous reports (von Waechter and Jaensch, 1972; Takahashi et al., 1995).

When 5AzC was injected with BrdU, BrdU-incorporated cells transitioned from S to G2/M phase during hours 1 through 3. At 6 h, more 5AzC-treated cells than control cells were still in G2/M (control, 16.5 ± 3.4%; 5AzC, 43.6 ± 6.7%). Many of these cells likely were in M phase because most of the abnormal mitotic cells were BrdU-positive in our previous study (Ueno et al., 2002a). At 9 h, most of them still remained in the G2/M phase (control, 5.3 ± 1.9%; 5AzC, 23.9 ± 2.7%), but some cells had moved to G0/G1. In our previous results, at 9 h, small number of BrdU-positive cells (about 4%) were mitotic cells

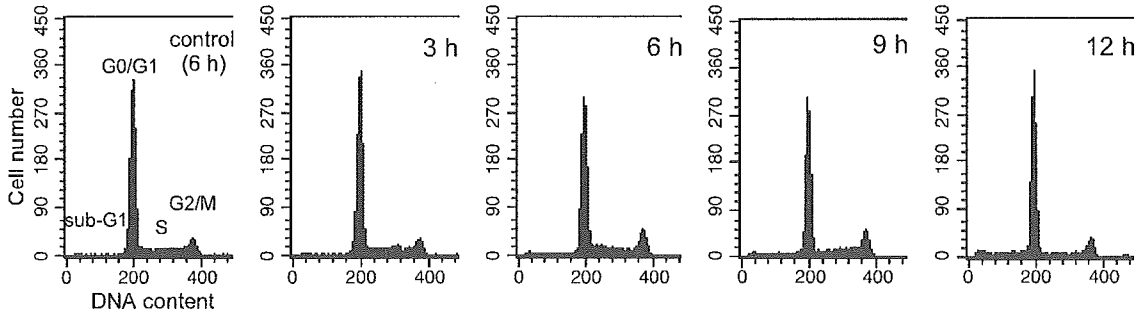

	control (6 h)	3 h	6 h	9 h	12 h
Sub-G1	0.6 ± 0.3 (%)	0.5 ± 0.1	5.0 ± 1.2*	7.0 ± 1.7*	15.8 ± 3.2*
G0/G1	72.5 ± 1.4	71.6 ± 0.2	61.6 ± 1.0*	56.6 ± 3.0*	63.2 ± 3.2*
S	18.1 ± 0.7	19.0 ± 0.8	18.3 ± 1.0	20.3 ± 1.7	10.8 ± 0.9*
G2/M	8.8 ± 0.7	8.9 ± 0.9	15.0 ± 0.9*	16.1 ± 0.6*	10.2 ± 0.3*

Fig. 2. Cell cycle analysis of telencephalic cells in the rat fetus (*x* axis: PI intensity (DNA content), *y* axis: cell number). Percentages for each cell cycle phase are presented as the mean ± SD of 3 dams. The treatment of 5AzC increased the number of G2/M cells from 6 to 9 h and apoptotic cells in the sub-G1 area from 6 to 12 h. *$P < 0.05$; significantly different from the control (6 h) (Student's *t* test).

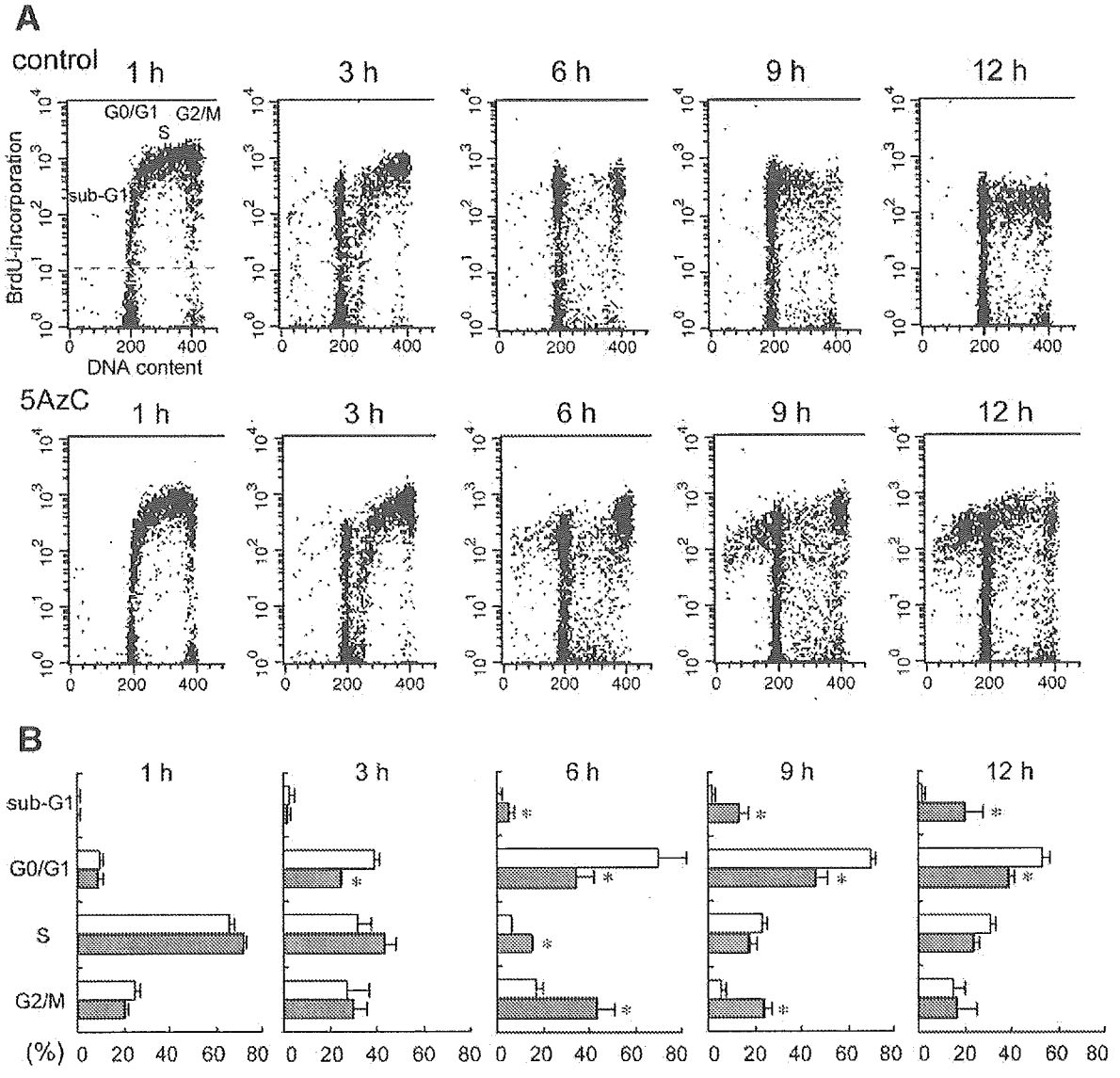

Fig. 3. Transition of BrdU-incorporated telencephalic cells of rat fetus in the cell cycle. (A) Detection of BrdU-incorporated cells in the cell cycle using flow cytometry (*x* axis: PI intensity (DNA content), *y* axis: FITC intensity (BrdU incorporation)). The cells that have FITC intensity above the dotted line are BrdU-positive cells. (B) Distribution of BrdU-positive cells in the cell cycle (white bar: control group, gray bar: 5AzC-treated group). Percentages for each cell cycle phase are presented as the mean ± SD of 2 dams. $^*P < 0.05$; significantly different from the control group (Student's *t* test). By 5AzC treatment, BrdU-positive cells were accumulated in G2/M phase from 6 to 9 h, and then they transited to G0/G1 or sub-G1 area (apoptosis).

(Ueno et al., 2002a), suggesting that G2 progression was inhibited in this period. Furthermore, some BrdU-positive cells had undergone apoptosis, as demonstrated by the increase in the sub-G1 area (13.3 ± 3.3%). At 12 h, the cells moved to G0/G1 or to the sub-G1 area, which contained apoptotic cells. These results indicate that cell cycle progression of 5AzC-treated neural progenitor cells was blocked in M phase at 6 h and in G2 phase at 9 h, after which the cells either entered G0/G1 phase or became apoptotic.

Cell cycle position of cells undergoing apoptosis

We then sought to confirm whether the 5AzC-treated apoptotic cells had died before or after mitosis. The results of our cell cycle analysis were consistent with those of our histopathological examination, showing that apoptotic cells began to increase at 9 h and that the number peaked at 12 h after 5AzC treatment (Ueno et al., 2002a,b, and Fig. 1C). To clarify at which cell cycle phase 5AzC-treated neural progenitor cells undergo cell death, we used flow cytometry to assess the presence of DNA strand breaks in cells versus their DNA content. The cells first were fixed with paraformaldehyde, which prevents apoptotic cells from losing their DNA fragments (loss of DNA fragments causes the cells to stain as a sub-G1 population) (Gorczyca et al., 1993; Murakami et al., 1995). In this way, the apoptotic cells with the DNA contents indicative of G0/G1, S, or G2/M phases can be detected, thus clarifying during which phase the cells died.

The results of the flow cytometric analysis of the paraformaldehyde-fixed cells are shown in Fig. 4. From 9 to

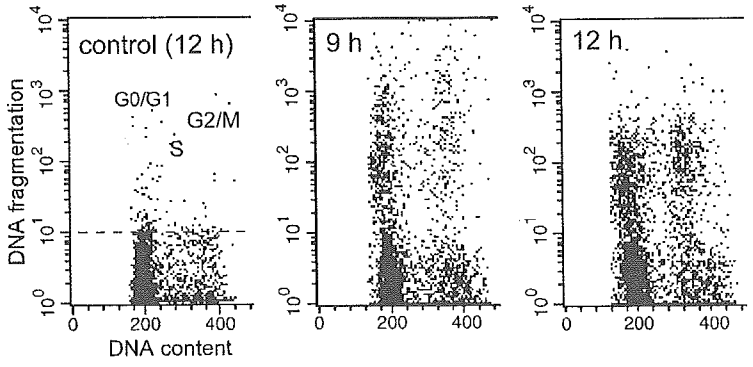

Apoptotic cell	1.8 ± 1.4 (%)	10.5 ± 3.6	19.5 ± 2.1
G0/G1	68.7 ± 5.4	65.0 ± 5.8	56.6 ± 3.7
S	18.4 ± 4.5	9.2 ± 1.5	9.6 ± 1.3
G2/M	12.9 ± 1.1	25.8 ± 4.9	33.8 ± 4.9

Fig. 4. Apoptotic cells and their DNA content in 5AzC-treated rat fetal telencephalon (*x* axis: PI intensity (DNA content), *y* axis: FITC intensity (DNA fragmentation)). The cells that have FITC intensity above the dotted line are BrdU-labeled apoptotic cells. Percentages of apoptotic cells and their cell cycle distribution are presented as the mean ± SD of 3 dams. 5AzC-induced apoptosis mainly occurred in G1, while also in G2/M and S phase.

12 h after the treatment, most of the cells undergoing apoptosis were in G0/G1 phase (9 h, 65.0 ± 5.8%; 12 h, 56.6 ± 3.7%), although some were in G2/M and S phases. At 12 h, the ratio of apoptotic cells in the G0/G1 phase decreased and that in the G2/M phase increased slightly. The current findings suggest that apoptosis predominantly is induced after the mitosis, but some cells die before. These results are consistent with our previous report, which showed that some neural progenitor cells underwent apoptosis after mitosis (Ueno et al., 2002a).

p53 and G2/M checkpoint proteins

In our previous study, we suggested that p53 and its transcriptional target genes play important roles in 5AzC-induced toxicity in the neural progenitor cells (Ueno et al., 2002a). In addition, the present cell cycle analysis further demonstrated that 5AzC inhibited G2/M progression. Therefore, we focused on p53 and cell cycle regulators in G2/M phase and examined the expression of these proteins.

The expression of p53 protein was elevated during hours 6 through 12 (Fig. 5A), a finding consistent with our previous immunostaining results (Ueno et al., 2002a). The expression of $p21^{waf1/cip1}$, a CDK inhibitor and target gene of p53, also increased (Fig. 5A). We therefore examined cell cycle alteration in p53-knockout mice to confirm the influence of p53 on the cell cycle and apoptosis. Histopathological evaluation revealed abnormal accumulation of mitotic cells along the ventricle at 6 h in every p53 genotype (Figs. 5B-a to c), suggesting that mitotic progression was blocked. These mitotic cells were positive for phospho-histone H3 (Figs. 5B-g to i). At 12 h, pyknotic cells positive for cleaved caspase-3 were observed in the $p53^{+/+}$ (wild-type) and $p53^{+/-}$ mice, but not in the $p53^{-/-}$ mice (Figs. 5B-d to f and j to l). In the cell cycle analysis (Fig. 5C), the number of G2/M cells increased in every genotype at 6 to 12 h (6 h; +/+, 15.7 ± 1.0%; +/−, 14.4 ± 1.9%; −/−, 14.2 ± 0.7%, 12 h; +/+, 13.8 ± 3.0%; +/−, 16.9 ± 3.4%; −/−, 19.1 ± 2.9%). The number of mitotic cells decreased in every p53 genotype at 12 h (Figs. 5B-d to f) compared to that at 6 h (Figs. 5B-a to c), while the number of G2/M cells increased at 12 h, suggesting that G2 progression was blocked at 12 h. At 12 h, the number of apoptotic cells in the sub-G1 area increased only in the $p53^{+/+}$ and $p53^{+/-}$ mice (+/+, 21.2 ± 6.3%; +/−: 11.2 ± 3.1%; −/−, 2.8 ± 1.5%). $p53^{-/-}$ neural progenitor cells escaped from apoptosis at 12 h, although the number of cells in the G2/M phase increased through the 6- and 12-h time points. These results suggest that 5AzC-induced apoptosis is p53-dependent and that the associated M and G2 block are p53-independent. Although S phase accumulation also occurred at 6 to 12 h in the $p53^{+/+}$ animals (Fig. 5C; 6 h, 16.8 ± 3.1%; 12 h, 13.2 ± 2.2%), it occurred only at 6 h in the $p53^{-/-}$ mice (Fig. 5C; 6 h, 15.2 ± 0.8%; 12 h, 6.4 ± 1.8%). Therefore, p53 may play a role in maintaining the inhibition of S-phase progression.

We then undertook DNA microarray analysis to seek the key factors in the regulation of cell cycle. According to the criteria described in Materials and methods, 249 genes were extracted. The expression of some target genes of p53 (*$p21^{waf1/cip1}$*, *cyclin G1*, *Igfbp3*, *Mdm2*, *Snk*) was upregulated from 6 to 12 h (Table 1). In addition, the expression of some genes involved in the cell cycle regulation was also changed from 6 to 12 h (Table 1).

In the pathway analysis, we noted enhanced expression (mainly at 12 h) of two genes regulating the G2/M transition (*cyclin B1* and *Cdc20*) (Fig. 6A). We confirmed the increased mRNA expression of these genes by using real-time PCR (Fig. 6B). In light of the results in the $p53^{-/-}$ fetal brain and elevated mRNA expression of the genes regulating the G2/M transition, we focused on the p53-independent cascade regulating G2/M transition, and we used Western blotting to examine the expression of cyclin B1, Cdc2 (Cdk1), phospho-Cdc2 (Tyr16), and Chk2 protein (Fig. 6C). Expression of cyclin B1 increased from hours 3 to 9. The amount of phosphorylated Cdc2 was lowest at 6 h and gradually increased from 9 to 12 h, whereas the expression of Cdc2 was nearly unchanged throughout the

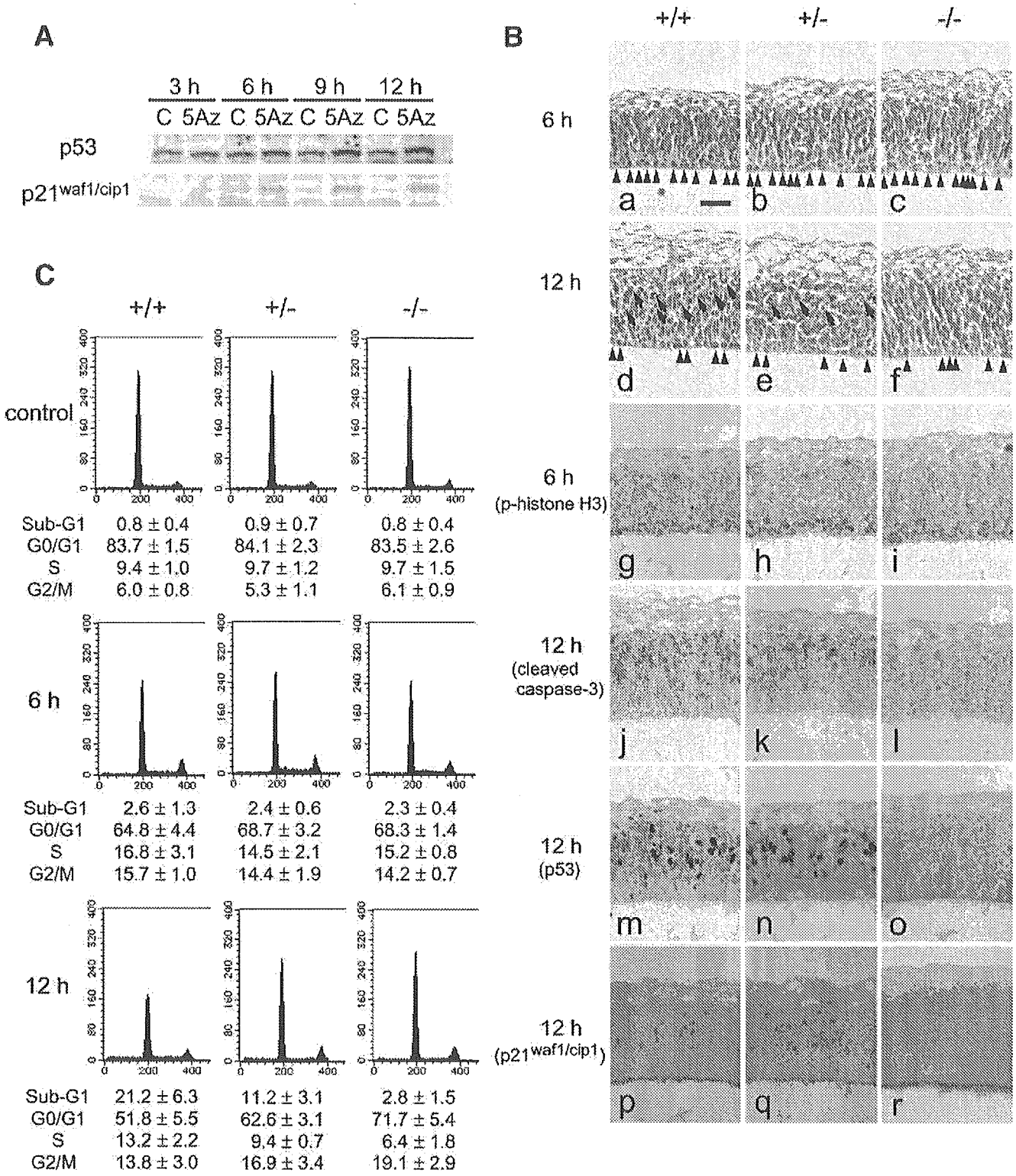

Fig. 5. 5AzC-induced p53-dependent apoptosis and p53-independent G2/M arrest. (A) Western blot analysis of p53 and $p21^{waf1/cip1}$ in control (C) and 5AzC-treated (5Az) rat fetal telencephalon. The expression of p53 and its target gene, $p21^{waf1/cip1}$, increased from 6 to 12 h. (B) Histopathological changes in the VZ of dorsal telencephalic wall of p53-knockout mice fetus. (a–f) Hematoxylin and eosin staining. (g–i) Phospho-histone H3 at 6 h. (j–l) Cleaved caspase-3 at 12 h. (m–o) p53 staining at 12 h. (p–r) $p21^{waf1/cip1}$ staining at 12 h. Accumulation of mitotic cells is observed in every p53 genotype (a–c and g–i, arrowheads: mitotic cells) and then decreased at 12 h (d–f, arrowheads: mitotic cells). Apoptosis is induced in $p53^{+/+}$ and $p53^{+/-}$ mice, but not in $p53^{-/-}$ mice (d–f and j–l, arrows: apoptotic cells). p53 and $p21^{waf1/cip1}$ are expressed in $p53^{+/+}$ and $p53^{+/-}$ mice, but not in $p53^{-/-}$ mice (m–o and p–r). Scale bar: 50 μm. (C) Cell cycle analysis of telencephalic cells of p53-knockout mice fetuses (x axis: PI intensity (DNA content), y axis: cell number). Percentages for each cell cycle phase are presented as the mean ± SD of 3 dams. In $p53^{+/+}$ and $p53^{+/-}$ mice, the number of G2/M phase cells increased at 6 h and apoptosis in the sub-G1 area at 12 h. In $p53^{-/-}$ mice, the number of G2/M phase cells increased from 6 to 12 h, but apoptosis did not occur remarkably.

Table 1
Expression changes of cell-cycle-related genes in the rat fetal telencephalon treated with 5AzC

Accession no.	Genes	Fold change		
		6 h	9 h	12 h
Cell cycle				
NM_022183.1	topoisomerase (DNA) II alpha (Top2a)		1.33 ± 0.09	
U05341.1	Cdc20/p55CDC			1.52 ± 0.09
X64589.1	cyclin B (Ccnb1)			1.40 ± 0.16
NM_012760.1	lost on transformation 1 (Lot1)/pleiomorphic adenoma gene-like 1 (Plagl1)/Zac1	−1.17 ± 0.05		
NM_054008.1	rgc32 protein (Rgc32)			−1.98 ± 0.47
NM_022683.1	vasopressin-activated calcium-mobilizing receptor protein (VACM-1)/cullin-5 (Cul5)			−1.77 ± 0.72
NM_021662.1	DNA polymerase delta, catalytic subunit (Pold1)			−1.52 ± 0.17
NM_017258.1	B-cell translocation gene 1, anti-proliferative (Btg1)			−1.37 ± 0.2
p53-target genes				
NM_012923.1	cyclin G1 (Ccng1)	1.93 ± 0.00	3.02 ± 0.38	3.23 ± 0.03
U24174.1	p21 (Waf1/Cip1)		4.10 ± 2.77	
BF548539	ESTs, Moderately similar to S15349 mdm2 protein-mouse (*M. musculus*)		1.63 ± 0.04	
NM_031821.1	serum-inducible kinase (Snk)/Plk2		1.42 ± 0.19	
NM_012588.1	insulin-like growth factor-binding protein (Igfbp3)		2.30 ± 0.98	1.86 ± 0.32

Fold change is presented as the mean ± SD of 2 arrays.

experimental period. The expression and mobility of Chk2 protein did not change through the experimental period.

Discussion

We showed that neural progenitor cells underwent G2/M accumulation and apoptosis due to 5AzC-induced stresses in the fetal CNS. Apoptosis likely is induced by a p53-dependent mechanism, and G2/M block probably occurs in a p53-independent manner.

5AzC is a cytidine analogue and has a DNA demethylating effect on cells. Incorporation of 5AzC into the CpG island of the DNA promoter region leads to exchange of deoxycytidine for 5AzC, and this exchange blocks DNA methylation. As mentioned before, in the developing brain, DNA methylation is a key step for regulating gene expression (Sun et al., 2003). Therefore, 5AzC may disturb gene expression and alter organogenesis through its DNA demethylating effect. In our DNA microarray analysis, it failed to identify any gene whose expression was upregulated by the demethylating effect, although only a few genes currently are known to transcriptionally regulate by DNA methylation in the developing brain. For example, the astroglial markers GFAP and S100β are hypermethylated in the early to mid developing brain before glial cells are produced (Sun et al., 2003; Takizawa et al., 2001; Namihira et al., 2004); however, their expression was unchanged at 6 to 12 h after 5AzC treatment (data not shown). Therefore, we were unable to definitively determine the role of 5AzC-induced demethylation in neural progenitor cells of the developing brain.

5AzC also acts as a DNA-damaging agent. When 5AzC or 5-aza-2′-deoxycytidine, which has deoxyribose instead of the ribose of 5AzC, is incorporated into DNA, it forms a covalent bond with DNA methyltransferase (Santi et al., 1984; Michalowsky and Jones, 1987; Ferguson et al., 1997), resulting in DNA damage (Juttermann et al., 1994; Karpf et al., 2001). Indeed, elevated expression of p53, known as a 'guardian of the genome', has been documented to occur after 5AzC or 5-aza-2′-deoxycytidine treatment (Karpf et al., 2001; Zhu et al., 2004). p53 plays a key role in DNA repair, cell cycle arrest, and apoptosis in response to DNA damage caused by irradiation, chemical treatments, and so on (May and May, 1999).

In our previous and present studies, we confirmed that p53 expression was augmented at the protein level in neural progenitor cells (Ueno et al., 2002a, and Figs. 5A, B-m) and that the expression of some target genes of p53 (*$p21^{waf1/cip1}$*, *cyclin G1*, *Igfbp3*, *Mdm2*, and *Snk*) was upregulated (Ueno et al., 2002a and Table 1). We therefore surmise that 5AzC exerts a toxic effect via DNA damage. However, in some contexts, such as loss of DNA methyltransferase, disturbance of the methylation state of the DNA from its normal pattern causes elevated p53 expression and cell death (Jackson-Grusby et al., 2001). Therefore, we cannot exclude the possibility that the toxicity of 5AzC is associated with a DNA demethylating effect.

We have shown that 5AzC induces a p53-dependent apoptosis (Figs. 5B and C), although the mechanism by which 5AzC activates p53 remains obscure. In contrast, the 5AzC-associated G2/M accumulation seems to be p53-independent. In the microarray and signal pathway analyses, the expression of genes that promote G2/M transition (*cyclin B1* and *Cdc20*) was upregulated (Figs. 6A and B), so we investigated an alternative pathway of cell cycle regulation. For the G2 to M transition, the activation of Cdc2 kinase (Cdk1) and its interaction with cyclin B1 are indispensable. Chk1 and Chk2 are serine kinases, which

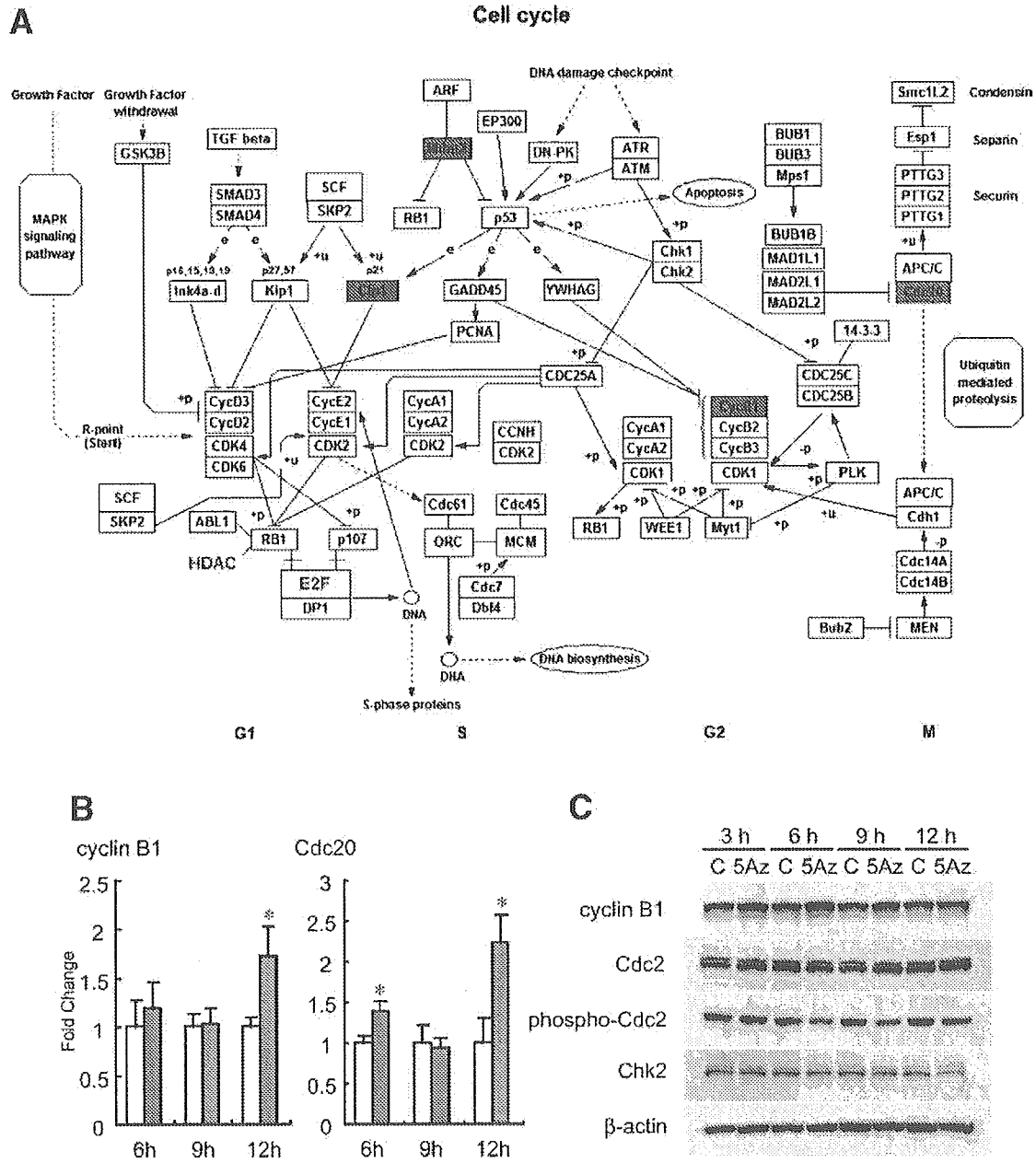

Fig. 6. Changes in the expression of G2/M phase regulators in 5AzC-treated rat fetal telencephalon. (A) The cascade of cell cycle regulation showed by GenMAPP. Red labeled genes are the upregulated genes by 5AzC treatment. They are p53-related genes ($p21^{waf1/cip1}$ and *Mdm2*) and G2/M regulating genes (*cyclin B1* and *Cdc20*). On the other hand, there are no downregulated genes. (B) mRNA expression of G2/M regulating genes, *cyclin B1* and *Cdc20*, were examined by real-time PCR. The expression of both genes was upregulated at 12 h. $*P < 0.05$; significantly different from the control group (Student's *t* test). (C) Western blot analysis of G2/M phase regulators of control (C) and 5AzC-treated (5Az) rat fetal telencephalon. The expression of cyclin B1 increased slightly from 3 to 9 h and that of phosphorylated Cdc2 (Tyr16) decreased from 6 to 12 h, suggesting the abnormal activation of G2 to M transition. The expression and mobility of Chk2 did not change through the experimental period.

are activated in response to DNA damage (Chaturvedi et al., 1999; Liu et al., 2000; Matsuoka et al., 2000) and lead to G2 arrest through inactivation of Cdc2. The Cdc2–cyclin B complex becomes inactive after phosphorylation of tyrosine 15 and threonine 14 of Cdc2. Cdc25 dephosphorylates and activates Cdc2, but Chk1 and Chk2 phosphorylate and sequester Cdc25 in the cytoplasm, where it is ineffective. As a result, Cdc2 becomes phosphorylated and inactive. In some G2 arrest models, the arrest is reported to be brought about by Chk1 or Chk2, independent of p53 (Taylor and Stark, 2001; Iliakis et al., 2003).

However, in the present study, phospho-Cdc2 decreased, although G2 progression was blocked (Fig. 6C). This abnormal activation of Cdc2 might accelerate the G2 to M transition, probably resulting in accumulation of mitotic cells. Furthermore, the expression of cyclin B1 was slightly increased at 3 to 9 h (Fig. 6C). Cyclin B1 is degraded by anaphase-promoting complex (APC) at metaphase, and this process is indispensable for mitotic progression, so the accumulation of cyclin B1 that we observed might occur as a result of inactivation of APC, which leads to mitotic arrest (Nitta et al., 2004). The mitotic